

1 **Subseasonal atmospheric variability and El Niño waveguide warming;**  
2 **observed effects of the Madden-Julian Oscillation and Westerly Wind Events.**

3  
4  
5  
6  
7 Andrew M Chiodi

8 Joint Institute for the Study of the Atmosphere and Ocean, University of Washington, and  
9 NOAA Pacific Marine Environmental Laboratory

10  
11  
12  
13 Don E. Harrison

14 Joint Institute for the Study of the Atmosphere and Ocean, University of Washington, and  
15 NOAA Pacific Marine Environmental Laboratory

16  
17  
18 Gabriel A. Vecchi

19 Geophysical Fluid Dynamics Laboratory, Princeton University  
20  
21  
22  
23  
24  
25  
26  
27  
28

29 <sup>1</sup> *Corresponding author address:* Andrew Chiodi, NOAA PMEL, Box 354925, 7600 Sand Point Way N.E.  
30 Seattle, WA, 98115  
31 E-mail: [andy.chiodi@noaa.gov](mailto:andy.chiodi@noaa.gov)  
32  
33

34  
35  
36  
37  
38  
39  
40  
41  
42  
43  
44  
45  
46  
47  
48  
49  
50  
51  
52  
53  
54  
55  
56

## Abstract

Westerly Wind Events ("WWEs") have previously been shown to initiate and maintain equatorial Pacific waveguide warming. The relationship between WWE and intra-seasonal Oscillation (or Madden-Julian Oscillation; "MJO") activity, and the role of MJO events in initiating and maintaining equatorial Pacific waveguide warming is reconsidered here, over the time period 1986-2010. WWEs are identified in the observed record of near surface zonal winds based on an objective scheme. MJO events are defined using a widely used index, and 62 are identified over this period that occur when the El Niño-Southern Oscillation (ENSO) is in its neutral-state ( $|\text{NIÑO3}| < 0.75^\circ\text{C}$ ). 42 of these MJO events have one or more embedded WWEs and 20 have not.

We examine the time evolution of sea surface temperature anomaly over the Pacific equatorial waveguide following the westerly surface wind phase of the MJO over the western equatorial Pacific. We find that there is waveguide warming for the MJO+WWE events in similar magnitudes and amounts as following WWEs that are not embedded in an MJO, and that there is very little statistically significant waveguide warming following the MJO events that do not contain an embedded WWE. Further, we find that the occurrence of an MJO event does not significantly affect the likelihood that a WWE will occur. These results extend and confirm the results of Vecchi (2000) with a near doubling of the period of study. We suggest that understanding the sources and predictability of tropical Pacific Westerly Wind Events remains essential to improving predictions of the onset of El Niño events.

57

58

## 59 **1. Introduction**

60

61 Westerly Wind Events (WWEs) are zonal wind anomaly events in the western and central  
62 equatorial Pacific (Luther *et al.* 1983, Harrison and Giese 1991, Hartten 1996, Harrison and  
63 Vecchi 1997) with typical time, zonal-spatial and zonal-wind anomaly scales of 6 days, 6-7 ms<sup>-1</sup>  
64 (up to 15ms<sup>-1</sup> peak), and 1400-2500 km, respectively (Harrison and Vecchi 1997), that have been  
65 observed to occur during a wide range of atmospheric phenomena, including, tropical cyclones  
66 (both single and paired), cold-surges from the cold-hemisphere and convective activity  
67 associated with the Madden-Julian Oscillation, or ‘MJO’ (*e.g.*, Keen 1982, Harrison 1984, Love  
68 1985 a,b; Hartten 1996; Chen *et al.*, 1996; Lin and Johnson, 1996). WWEs with substantial wind  
69 anomaly in the western and central Pacific waveguide region (within a few degrees of the  
70 equator) have previously been shown to precede substantial (up to 1°C) equatorial Pacific cold  
71 tongue warming (Vecchi and Harrison 2000, Harrison and Chiodi, 2009) when the El Niño-  
72 Southern Oscillation (ENSO) is in neutral conditions, and maintain warm central/eastern Pacific  
73 sea surface temperature anomalies (SSTAs) in warm-ENSO conditions (Vecchi and Harrison  
74 2000). WWEs are rare in cool-ENSO conditions, in which case their effects are difficult to  
75 determine reliably (Vecchi and Harrison 2000).

76 Composite single WWE wind anomalies applied to ocean general circulation models (OGCMS)  
77 have been found to produce cold tongue warming on the order of 0.5°C (Giese and Harrison  
78 1990, 1991; Vecchi 2000; Lengaigne *et al.* 2002; Harrison and Chiodi 2009). There is general  
79 agreement that WWE-induced upper ocean advection anomalies are the primary cause of WWE-  
80 driven cold tongue warming. Zonal advection of the background zonal SST gradient has

81 typically been found to play a dominant role (Schopf and Harrison 1983; Harrison and Schopf  
82 1984; Kindle and Phoebus 1995; Giese and Harrison 1991), although some studies have also  
83 found different types of oceanic advection anomalies, including those associated with tropical  
84 instability wave modulation of meridional advection (Giese and Harrison 1991) and subsurface  
85 advection anomalies (Richardson et al. 1999; Belamari et al. 2003) to be of central importance.

86 The full role of WWEs in waveguide SST changes has been found to involve coupled ocean-  
87 atmosphere dynamical processes, with WWE-driven equatorial Pacific waveguide warming  
88 acting to enhance the probability of WWEs (Perigoud and Cassou 2000; Lengaigne *et al.* 2003;  
89 Lengaigne *et al.* 2004; Vecchi *et al.* 2006; Gebbie *et al.* 2007). Thus, the influence of WWEs on  
90 ENSO is enhanced by their dependence on the state of the tropical Pacific: WWEs are not best  
91 thought of as additive noise to the state of the tropical Pacific (*e.g.*, Lengaigne *et al.* 2004;  
92 Vecchi *et al.* 2006; Eisenman et al. 2005; Gebbie et al. 2007; Gebbie and Tziperman, 2009.a,b).  
93 Applied with frequency and number consistent with recently observed El Niño years, (multiple)  
94 WWEs have been shown to drive El Niño-like SSTAs (*e.g.* sustained seasonal ENSO index  
95 magnitudes of about 2°C) in realistic ocean circulation models (Harrison and Chiodi 2009).

96 MJO events are characterized by wind (among other) anomalies that propagate eastward at  
97 roughly 5 m s<sup>-1</sup>, oscillate in the 30-90 day period range, have zonal scales typical of low-  
98 atmospheric wavenumber phenomena, and include significant (~1.5 m s<sup>-1</sup> average), easterly and  
99 westerly surface wind anomalies over the equatorial Pacific waveguide (Madden and Julian,  
100 1972). Some have previously hypothesized that MJO events are important to the development of  
101 El Niño events because of their possible connection to WWEs (*e.g.* Slingo et al. 1999; Seiki et al.  
102 2007), while others have taken the view that surface wind stress variability characteristic of the  
103 MJO itself is important to the initiation and maintenance of El Niño-type tropical Pacific SSTAs.

104 For example, based on OGCM and coupled ocean-atmosphere model results, Kessler and  
105 Kleeman (2000) have proposed that MJO-like wind stresses in the western and central equatorial  
106 Pacific drive SSTA patterns in the western (cooling of about  $-0.4^{\circ}\text{C}$ ) and eastern (warming of  
107 about  $+0.1^{\circ}\text{C}$ ) equatorial Pacific that are conducive to the development of an El Niño event.  
108 Kessler (2001) found evidence that an extension of MJO-driven surface wind anomalies over the  
109 open waters of the western and central equatorial Pacific occurs during El Niño years, which was  
110 postulated to enhance the proposed rectification process. Seiki et al. (2009) have also postulated  
111 that changes associated with the development of El Niño events cause the MJO-associated  
112 surface winds to contribute further to El Niño-development. Alternatively, a perspective has  
113 developed over the last decade that argues that the MJO contains a “low frequency tail” (Zavala-  
114 Garay *et al.*, 2003), that is correlated with interannual anomalies of MJO variability (Zavala-  
115 Garay *et al.* 2005, 2008), and is important to the development of eastern equatorial Pacific (e.g.  
116 NIÑO3 region) SSTA anomalies (Kapur *et al.* 2011; see also Zhang and Gottshalck 2002).  
117 Within this body of literature, it has been claimed that the effects of MJO wind stress anomalies  
118 in tropical Pacific SSTA variability dominate those caused by WWEs because “those wind bursts  
119 associated with the MJO are of most importance for interaction with the ocean ENSO, as a large  
120 oceanic response is only driven by wind events that are spatially and temporally coherent”  
121 (Hendon *et al.* 2007).

122 Which is it? Do WWEs or MJO events help initiate El Niño events? And what is the relationship  
123 between WWEs and the MJO; does the state of the MJO influence the probability of seeing a  
124 WWE? To answer these questions we analyze the historical records of subseasonal wind and  
125 SST anomaly in the 1986-2010 period, identifying the times with WWEs and MJO events, and  
126 examining the changes in equatorial Pacific SSTA that follow them. The relative numbers of

127 WWEs that occur during and not during MJO-events, as well as the numbers of MJO events that  
128 do and do not contain a WWE are also analyzed in the context of a bootstrap-Monte Carlo  
129 simulation to determine whether there are statistically significant relationships between the  
130 timings of these two classes of subseasonal wind events.

131 Our main focus is on SSTA-changes following events that occur in ENSO-neutral conditions  
132 [here defined as in Vecchi and Harrison (2000) as  $|\text{NIÑO3}| < 0.75^\circ\text{C}$ ], since we are interested,  
133 inherently and for forecasting purposes, in the processes capable of initiating or at least  
134 influencing a transition to the warm-ENSO state. The results of our study are organized as  
135 follows. Composites of equatorial Pacific SSTA-changes following MJO and WWEs are  
136 examined in sections 3 and 4. Results from companion ocean general circulation model  
137 (OGCM) experiments, in which the model-ocean is forced with representative WWE and MJO  
138 wind stress anomalies, are compared in section 5. Results from a Monte Carlo-bootstrap  
139 examination of the MJO and WWE co-occurrence statistics are examined in section 6, and a  
140 discussion and conclusions are offered in section 7.

141

## 142 **2. Data and Methods**

143 For information on SST variability, we use NOAA Optimum Interpolation SST (OISST) V2  
144 provided by the NOAA/OAR/ESRL PSD, Boulder, Colorado, USA, from their Web site at  
145 <http://www.esrl.noaa.gov/psd/>. OISST data is available on a 1x1 degree grid at weekly  
146 resolution. For this study, this data is interpolated to daily resolution to estimate the changes in  
147 SSTA that occur over various subseasonal timescales (as described below). SST anomalies are  
148 determined using the climatological monthly mean values (base period 1986-2010), linearly

149 interpolated to daily resolution. The same 25 year base period is used to determine climatological  
150 means (and thereby anomalies) throughout this study.

151 We use wind data from the 12-hourly, 2.5 by 2.5 degree ECMWF operational forecast 10-m data  
152 set (as done in Chiodi and Harrison, 2009), which is available online at

153 <http://www.ecmwf.int/products/data> (provided at handling costs for research purposes).

154 The state of the MJO is determined using the now commonly referred to index suggested by  
155 Wheeler and Hendon (2004; WH04, hereafter), which is based on a pair of empirical orthogonal  
156 functions of the combined fields of near-equatorially averaged 850-hPa zonal wind, 200-hPa  
157 zonal wind and satellite-based outgoing longwave radiation data, is available at daily resolution  
158 from <http://www.cawcr.gov.au/staff/mwheeler/maproom/RMM/>. By convention, the MJO is  
159 considered active when the index amplitude is  $> 1$  and inactive when not. We identify “MJO-  
160 events” from this daily index as those intervals in the 1986-2010 period for which the MJO-  
161 amplitude is  $> 1$  for at least 20 consecutive days. Wind anomaly composites during these “MJO-  
162 active” times are shown in Appendix A for each of the 8 phases specified by the index, and  
163 reveal that statistically significant wind anomalies are seen over the tropical Pacific in each case.  
164 We chose to use the 20-consecutive-day requirement since it seemed prudent to focus our  
165 consideration on MJO events that reach some basic level of maturity relative to the timescale  
166 ( $\sim 30$ -90 day) commonly understood to characterize the MJO. Trial showed that this requirement  
167 can be omitted without significantly affecting the wind anomaly composite results discussed  
168 here. Other results, such as the total number of identified MJO events, are obviously influenced  
169 at least somewhat by this requirement, but the conclusions reached regarding the relationship  
170 between the MJO, WWEs and tropical Pacific waveguide warming are not dependent on it.

171 We also report on a second set of results, which, rather than using the WH04 index, instead  
172 identify MJO events according to the more traditional Maloney and Hartmann (1998) methods.  
173 In this case, a separate MJO index is constructed from the principal components of the first and  
174 second empirical orthogonal functions (PC1, PC2) of 20-80-day band-passed-filtered 850-mb  
175 zonal wind, averaged from 5°S to 5°N around the equator. This index is (with “t” time in  
176 pentads);

$$177 \text{Index}(t) = \text{PC1}(t) + [\text{PC2}(t + 2) + \text{PC2}(t + 3)]/2.$$

178 According to this methodology, MJO events are defined as periods in which > 1 standard  
179 deviation index-peaks are found to be both preceded and followed by index-troughs. The MJO  
180 phases (1-9 in this case) are assigned as follows; phase 5 occurs during the index-peak, whereas  
181 phases 1 and 9 are the preceding and subsequent troughs. Phases 3 and 7 are the increasing and  
182 decreasing zero-crossings, respectively, and the even-numbered phases are assigned such that  
183 they are evenly spaced between the odd-numbered phases. Thus, by definition in this case, each  
184 identified MJO event includes phases 1-9, with the latter phases (i.e. 7, 8, 9) being associated  
185 with surface westerlies over the western and central Pacific. Unless noted otherwise, however,  
186 the results presented below are based on the primary WH04-based MJO-event definition.

187 The WWE identification and compositing method used here was developed by Harrison and  
188 Vecchi (1997) and used previously by Vecchi and Harrison (2000) and Harrison and Chiodi  
189 (2009). This method defines WWE events based on three equatorial (5°S to 5°N) regions, with  
190 boundaries at 130°E-155°E, 155°E-180° and 180°-150°W, for the so-called W-, C- and E-type  
191 WWEs, respectively. WWEs are defined as any interval of 3 or more consecutive days for  
192 which the respective WWE-region average zonal wind anomaly exceeds  $2 \text{ m}\cdot\text{s}^{-1}$ . Event



193 composites are based on the identification of a center-day (Day 0), defined as the event-day with  
194 the maximum zonal wind anomaly (see Harrison and Chiodi, 2009 for more details). For  
195 reference, W-, C-, and E-type WWE composite wind anomalies for all events identified during  
196 the 1986-2010 period are shown in Appendix A.

197 To examine the effects of the MJO and WWEs on SSTA, we have compiled a data set consisting  
198 of the observed SSTA changes following each type of event in the 1986-2010 period. For  
199 WWEs, changes in SSTA are determined relative to the conditions seen 20 days prior to WWE  
200 Day 0. For consistency, changes following MJOs are determined 20 days prior to the first day  
201 that a given MJO event, as defined above using the WH04 index, reaches phase 6 (7 when based  
202 on the Maloney and Hartmann definition), the phase at which surface westerlies begin to  
203 dominate the MJO-composite wind anomalies in the tropical Pacific (see Appendix Figure A1).  
204 In each case, changes in SSTA at various time lags (e.g. +20, 40, 60 and 80 days) are composited  
205 over the events identified to occur in ENSO-neutral conditions. ENSO-neutral conditions are  
206 defined herein following Harrison and Chiodi (2009) and Vecchi and Harrison (2000), as the  
207 times in which the NIÑO3 index (SSTA averaged over the 150°W-90°W, 5°S-5°N region) has  
208 amplitude less than 0.75°C (i.e.  $|\text{NIÑO3}| < 0.75^\circ\text{C}$ ).

209 The statistical significances of the composite SSTA-changes are determined using a Monte-Carlo  
210 bootstrap procedure, in which random selection (with replacement) from the 1986-2010 record  
211 of all possible ENSO-neutral SSTA changes is used to estimate the probability that the  
212 magnitude of a given composite SSTA-change can be explained by the effects of random  
213 selection. The Monte-Carlo procedure is explained more in Appendix B.

214 The ocean model used herein is based on the longstanding NOAA primitive equation OGCM  
215 (e.g. Philander and Siegel, 1985). The configuration used here, based on NOAA's Geophysical  
216 Fluid Dynamics Laboratory Modular (GFDL) Ocean Model (version MOM4; Griffies *et al.*  
217 2003). The global version of MOM4 is the oceanic component of the GFDL Coupled Model 2  
218 (Gnanadesikan et al. 2006), and a tropical Pacific version of the model has been used recently to  
219 successfully describe the seasonal cycle of the near surface tropical Pacific by Harrison et al.  
220 (2009) and to study the effects of WWE wind stress anomalies by Harrison and Chiodi (2009).  
221 To force the experiments described herein, wind data are converted to zonal psuedostress ( $\tau^x$ )  
222 using the following formula (as done in Harrison and Chiodi 2009),

$$223 \quad \tau^x = \rho_a C_d |U| u$$

224 Here, air density ( $\rho_a$ ) is assigned the value of  $1.25 \text{ kg m}^{-3}$ ,  $C_d$  is assumed to have the value of  $1.3$   
225  $10^{-3}$ ,  $|U|$  is the magnitude of the 10-m wind vector and  $u$  is its zonal component.

226 To examine the effects of MJO wind stress anomalies on tropical Pacific SST, pseudo-event  
227 wind stress anomalies are formed from the sequence of MJO-phase composites (1 through 8).  
228 Each phase is prescribed to last 5 days, for a total of 40 days of anomaly forcing. Wind stress  
229 anomalies are applied to the model beginning with phase 1. The effects of using a different  
230 starting point (e.g. start with phase 6 and proceed in modulo order) were examined but are not  
231 discussed since they produce results qualitatively similar to those described herein. We have  
232 also experimented with prescribing the duration of the phase according to the actual time spent in  
233 each in the identified MJO events, but find results qualitatively similar to those produced by the  
234 5-day duration composites are yielded in this case (as described in the results section).

235 For comparison, the effects of WWE-type wind stress anomalies are also examined with OGCM  
236 experiments following the methods of Harrison and Chiodi (2009), in which case the respective  
237 daily WWE-wind stress anomaly composites from event-day -20 to +20 are applied to the model.  
238 In both the MJO and WWE experiments, the model is first spun up to realistic climatological  
239 conditions (as described in detail in Harrison et al. 2009), and the wind stress-driven SSTAs are  
240 determined by comparing the model SST fields produced by integrating the model with and  
241 without the respective wind stress anomalies.

242

### 243 **3. Observed SSTA changes following MJO events**

244 We identified 62 MJO events that occurred in the 1986-2010 period during ENSO-neutral  
245 conditions and lasted at least 20 days, the vast majority of which (58) reached their westerly  
246 surface phase (i.e. phases 6, 7, and 8). The composite change in SSTA following these 58 MJO  
247 events, keyed on the beginning of the westerly surface phase (phase 6), are shown in the left-  
248 hand-side panels of Figure 1, with shading where the composited SSTA-changes are statistically  
249 significant ( $p > 0.95$ ) based on Monte-Carlo bootstrap methods. The composite SSTA-change  
250 20 days after the start of MJO phase 6 (upper left panel) shows little statistically significant  
251 anomaly that persists to the following +40 day composite, which, like the +20 day case, shows  
252 rather little change from starting conditions in the tropical Pacific. The subsequent +60 day  
253 composite shows some warming in the eastern equatorial Pacific between 140°W and 100°W  
254 with amplitudes of 0.2-0.4°C, which are not yet statistically significant. This warming pattern  
255 intensifies by the +80 day composite, however, becoming statistically significant then.

256 Of these 58 MJO events, 41 have an embedded WWE, and 17 do not. The composite changes in  
257 SSTA following MJOs without a WWE are shown in the middle column of Figure 1.  
258 Examination clearly shows that, in an average sense, statistically significant warming does not  
259 follow the 17 MJO events that do not contain a WWE.

260 On the other hand, the SSTA-changes that follow MJO events containing at least one W-, C-, or  
261 E-type WWE (right-hand-side panels of Fig. 1) produce some isolated regions of warming in the  
262 central equatorial Pacific in the day +20 composite, that can be seen to broaden to an elongated  
263 pattern of  $>0.2^{\circ}\text{C}$  warming located between the Dateline and about  $110^{\circ}\text{W}$  in the +40 and +60  
264 day composites, and continues to intensify as it moves eastward during the next weeks, resulting  
265 in substantial ( $0.4\text{-}0.6^{\circ}\text{C}$ ) and statistically significant warming in the eastern equatorial Pacific  
266 by the day +80 composite.

267 We also used the methods of Maloney and Hartmann (1998; MH98 hereafter) to identify 68  
268 MJO events that occurring in ENSO-neutral conditions during the study period. The  
269 corresponding day +80 composites of SSTA-change are shown in Figure 2 for the 47 MH98-  
270 identified MJO events that do and 21 Mh98-identified MJO events that do not contain a WWE.  
271 The corresponding +80 day WH04-based SSTA-change composites (as discussed above) are also  
272 shown in this figure for comparison. Based on the MH98 definition, very little equatorial  
273 Pacific warming is seen following the identified MJO events regardless of whether they do or do  
274 not contain a WWE.

275

#### 276 **4. Observed SSTA-change following WWEs**

277 Ninety-eight W-type WWEs are identified in the 1986-2010 period that occurred during ENSO-  
278 neutral conditions. The composite changes in SSTA that follow these WWEs are shown in the  
279 left-hand-column of Figure 3, where it can be seen that a small ( $< 0.2^{\circ}\text{C}$ ), but statistically  
280 significant warming occurs in the central equatorial Pacific in the first 20 days following these  
281 WWEs, that intensifies and moves eastward over the following weeks, resulting in a coherent  
282 pattern of equatorially trapped warming in the +80 day composite that spans much of the central  
283 and eastern equatorial Pacific and has amplitudes  $> 0.4^{\circ}\text{C}$  in the eastern equatorial Pacific.

284 The composite SSTA changes following C-type and E-type WWEs that occurred in ENSO-  
285 neutral conditions over the same 25-year period are shown in the middle- and right-hand column  
286 of Figure 3, respectively (based on 105 C-type WWEs and 52 E-type WWEs). Some differences  
287 and similarities between these and the W-type composite are evident. For example, the warming  
288 amplitudes following the C-type (E-type) events are somewhat smaller (larger) than seen in the  
289 W-type case, and the coherent cooling seen west of the Dateline in the W-type composites is not  
290 evident to the same degree in the C- and E-type composites. However, the same basic picture  
291 emerges from each of these three composite-sequences; in an average sense, warming anomalies  
292 with amplitudes of a few to several tenths of a degree C appear in the central and eastern  
293 equatorial Pacific following each of these three types of WWEs.

294 For reference, the +80 day changes in NIÑO3 that follow each of these types of WWEs are listed  
295 in Table 1. Results for all WWEs occurring in ENSO-neutral conditions show that on average,  
296 the NIÑO3 SSTA index warms by a statistically significant ( $p > 0.95$ ) few tenths of a degree C  
297 following each of these three types of WWEs (1<sup>st</sup> column). Results also show that warming is  
298 seen regardless of whether the WWEs occur during MJO-events (2<sup>nd</sup> column) or not (3<sup>rd</sup>

299 column), and although somewhat larger warming amplitudes were seen following the WWEs  
300 that occurred during MJO-events, especially in the E-type composite, the differences between  
301 these and the composite NIÑO3 changes following WWEs that did not occur during an MJO-  
302 event are not statistically significant at the 90% confidence level. At lower levels (e.g. 80%), the  
303 E-type difference, which is based on the fewest number of samples, may become statistically  
304 significant, but the differences seen for the W- and C- types remain well within the range  
305 expected from the effects of random selection (even at the 66% confidence level).

306

## 307 **5. Model response to composite MJO wind anomalies**

308 The effects of MJO wind stress anomalies applied to a realistic ocean general circulation model  
309 are examined in the experiments described here. In each experiment, we first formed composite  
310 wind stress anomalies for each phase of the MJO based on the daily anomalies seen in the  
311 identified MJO-events that occurred in ENSO-neutral conditions. Next we form a pseudo-  
312 MJO-event composite based on the 8 different phase-composites by prescribing that each phase  
313 lasts for 5 days. The resulting 40-day wind stress anomaly composite (shown atop Figure 4) is  
314 then applied to the model. We have also looked at what happens when the phase duration is  
315 specified according to the time spent, on average, in each phase during the identified MJO  
316 events, but found that the results are very similar to those produced by the 5-day phase  
317 composite (as discussed further, below).

318 Preliminary experiments showed that the model results remain qualitatively similar regardless of  
319 which season the wind stress composites are applied in. For brevity, we discuss results from a  
320 single case (June), in which the wind composites are applied during a season typically associated

321 with the El Niño “onset” stage (Larkin and Harrison, 2002). The conclusions reached herein are  
322 not affected by the choice of month in which the wind anomalies are applied to the model.

323 We discuss results from 3 different experiments that are procedurally similar except that in the  
324 first, all 62 ENSO-neutral MJO events that are identified using the WH04 index are used to form  
325 the pseudo-event composite. In the second, just those MJO-events with embedded W-, C-, or E-  
326 type WWEs are used. And in the third, only the MJO-events that do not contain a WWE are  
327 used.

328 The evolution of SSTA in the months following the application of the composite based on all of  
329 the 62 MJO-events that occurred in ENSO-neutral conditions is shown in the left-hand-side  
330 panels of Figure 5, where it can be seen that only relatively modest amplitude ( $< 0.2^{\circ}\text{C}$ ) changes  
331 in SST, are driven in the model and last until days +60 or +80 in this case.

332 The SSTAs driven by the composite based on MJO-events that do not contain any WWEs are  
333 shown in the middle-column of panels of in Figure 5, and the composite based on MJO-events  
334 that contain either a W-, C-, or E-type WWEs are shown in the panels on the right-hand-side of  
335 this figure. Comparison of these results reveals change in character depending on whether the  
336 original MJO events did or did not contain a WWE. The MJO wind stress composite with a  
337 WWE produces a patch of small amplitude ( $0.1\text{-}0.2^{\circ}\text{C}$ ) equatorially trapped warming near the  
338 Dateline that can be seen in the +40 day panel (right-hand column, 2<sup>nd</sup> row), which is followed  
339 by a somewhat stronger, albeit still relatively modest ( $0.2\text{-}0.4^{\circ}\text{C}$ ) patch of warming in the cold  
340 tongue region (e.g.  $\sim 140^{\circ}\text{W}$  to  $110^{\circ}\text{W}$ ) in the +60 and +80day panels (right-hand column,  
341 bottom two rows). In contrast, the experiment based on the MJO-events that do not contain a  
342 WWE (middle column of panels) does not show warming in these regions at these times.

343 Comparison with the companion SSTA-changes seen following MJO events in the observations  
344 show some differences and similarities in each case. In the 62-MJO-event case, the warming  
345 seen in the composite of observed SSTA changes (Fig. 1, left-hand-side) shows somewhat larger  
346 amplitude warming at +80 days compared to the model. This could be due to the aliasing of  
347 other sources of warming (e.g. previous WWEs), errors in the composite wind stress, or model  
348 biases. The observed SSTA changes following MJOs with WWEs (Fig. 1, right-hand column)  
349 shows a small patch of warming in the 110°W-100°W region in the +20 day composite that is  
350 not reproduced in the model (Fig. 5, right-hand-column), that could likewise be due to, for  
351 example, the effect of several prior but closely timed WWEs. Also, the cooling amplitudes seen  
352 in the model following a MJO-wind anomaly composite that does not contain a WWE (Fig. 5,  
353 middle-column), which peak in the 0.6-0.8°C range, are larger in magnitude (by about 0.2°C)  
354 and broader scale than the cooling seen in the companion +20 and +40 day observation-based  
355 SSTA-change composites (Fig. 1, middle-column). Even with these differences, however, the  
356 MJO model experiments and composite analysis have in common the fact that, in each case, the  
357 SSTA-changes that include the effects of WWEs lead to cold-tongue warming on the order of a  
358 few tenths of a degree following the wind event. The results for MJO events that do not contain  
359 a WWE, however, do not show this type of warming.

360 As mentioned above, we have also repeated the experiments discussed above after modifying the  
361 idealized MJO composite so that the number of days spent in phase varies (at 6 hour resolution)  
362 according to the average time spent in each phase in the identified MJO events. The average  
363 duration across all phases turns out to be 4.5 days, ranging from 5.5 days in phase 6 to 3 days in  
364 phase 4. Qualitatively similar results are obtained in the varying- and equal-duration cases (c.f.  
365 Appendix Figure C1). The character of SSTA produced in the model depends much more on



366 whether the MJO does or does not contain a WWE than it does on these types of details of the  
367 observed MJO phase-duration.

## 368 **6. Model response to WWE wind stress anomaly**

369 The SSTA anomalies driven in the ocean model by composite W-, C- and E-type WWE wind  
370 stress anomalies can be seen in Figure 6. As in the MJO base-case, the wind anomalies in these  
371 experiments are applied for 40 days. For each WWE type, equatorially trapped warming on the  
372 order of a few tenths of a degree C is seen following the WWE in the equatorial central Pacific  
373 and later in the equatorial eastern Pacific, at somewhat greater amplitude than seen earlier around  
374 the Dateline. It is notable that this set of composite wind stress anomalies, which is keyed  
375 specifically on WWEs rather than the MJO phases, drives warming patterns that are more  
376 coherent and larger than, but nonetheless similar in character to those driven in the model by the  
377 “MJO-with-WWE” wind stress composites. For example, in each case, an initial near-  
378 equatorial warming is seen around the Dateline (i.e. in the +20 or +40 day panels) that is  
379 followed (at +60 or +80 days) by stronger warming in the equatorial eastern central Pacific.  
380 Some differences are noticeable also. Less initial warming is seen in the MJO-with-WWE  
381 model experiments than is seen in the experiments that key specifically on WWEs, which  
382 perhaps is not surprising given that the applied MJO wind anomaly composite begins in its  
383 surface-easterly wind anomaly phase and such easterlies, which should be expected to cool the  
384 central and eastern Pacific, are not, in general, a characteristic of WWE wind anomalies.

385 That oceanic waveguide warming is seen in the model following the application of W-, C- and  
386 E-type wind anomaly composites, as well as the MJO+WWE composite, but not seen following  
387 the MJO-without-WWE wind anomalies shows that in these model experiments it is the WWE  
388 wind anomalies that drive cold tongue warming, not the MJO.

389  
390 Comparison of the WWE-based model (Fig. 6) and observational results (Fig. 3) reveals some  
391 similarities and differences. But keeping in mind the many possible reasons for discrepancies of  
392  $\sim 0.2^{\circ}\text{C}$  (e.g. wind stress error, model bias, aliasing SSTA changes caused by other events in the  
393 observations), it can be said that the upper ocean circulation changes driven in the model by the  
394 composite WWE wind anomalies cause warming of SSTA in the central and eastern equatorial  
395 Pacific that is at least roughly consistent in terms of magnitude, timing and character, with the  
396 changes observed to follow these types of WWEs in an average sense. This is consistent with  
397 results previously discussed by Vecchi and Harrison (2000) and Harrison and Chiodi (2009).

398  
399 We also looked at the effects of using WWE wind anomalies composited over just those WWEs  
400 that occurred and did not occur during an MJO-event, but found that very similar SSTAs were  
401 driven in each case. This can be seen in Figure 7, where the equatorial SSTA changes following  
402 the application of two C-type WWE composites (embedded in MJO and not) are shown in the  
403 time-longitude perspective. We also ran the corresponding W- and E-type experiments, and  
404 found that similarly small differences in SSTAs are seen in these cases between the MJO-  
405 embedded and not-embedded composites (not shown for brevity). The state of the MJO does  
406 not appear to importantly affect the ability of the WWEs to cause warming of the central and  
407 eastern equatorial Pacific.

## 408 7. Model diagnostics

409 In this section we further explore the oceanic processes that allow equatorially centered WWEs  
410 to warm the oceanic waveguide in the several months following their occurrence. We have

411 examined the model behavior following the application of each type of WWE discussed here (W,  
412 C, and E) and found qualitatively similar results in this case. Thus, we have chosen to present  
413 just one set of results here (the C-type), rather than unnecessarily lengthen the manuscript.

414 Panel (a) of Figure 8 shows, again in the time-longitude perspective, the equatorial upper ocean  
415 (0-50m and 2°S-2°N average) temperature anomaly that is produced in the model following the  
416 application of a C-type WWE wind anomaly. Panel (b) shows the result of integrating the sum  
417 of each of the terms in the model heat budget (e.g. horizontal and vertical advection of the  
418 temperature gradient, surface heat flux, diffusion, etc). The close correspondence between the  
419 temperature anomaly patterns shown in Panels (a) and (b) confirms that the terms we examine  
420 accurately represent the warming actually seen in the model. In Panels (c) and (d), the anomaly  
421 seen in Panel (b) is separated into two components; that driven by changes in ocean circulation  
422 (Panel c) and that produced by other processes (e.g. vertical diffusion) that we have chosen to  
423 sum after finding that the anomaly seen in Panel (a) is driven predominantly by the circulation  
424 changes. In Panels (e) through (h) we further examine these circulation anomaly effects. The  
425 temperature tendency that produces the anomaly seen in Panel (c), that is, the 1<sup>st</sup> derivative of the  
426 advection-driven temperature anomaly, is shown in Panel (e). In Panels (f) and (g) this  
427 temperature tendency is split into parts driven by horizontal and vertical changes in circulation,  
428 respectively. This reveals that the horizontal and vertical advection terms (specifically the  
429 horizontal and vertical heat flux divergence anomalies) are each much larger in amplitude than  
430 the net temperature tendency seen in the model, but have very similar oppositely-signed patterns.  
431 Thus, the warming seen in the model results from there being a small imbalance between these  
432 two much larger, nearly-compensating terms. To more clearly gauge which component  
433 drives/damps the net change in temperature, in Panel (h) we have shaded the time-and-space

434 where there is  $> 0.015$  °C/day-amplitude net warming. The shading hue and value is chosen as  
435 follows: red if warming  $>$  cooling, blue otherwise; dark if horizontal  $>$  vertical, light otherwise.  
436 We thereby see that the initial (June-July) near-Dateline warming occurs because the horizontal  
437 (warming) component dominates the vertical (cooling) component then. The resulting warm-  
438 SSTA in this location then subsides mainly because of the effects of vertical (cooling) advection.  
439 Further east, the larger-amplitude warming that occurs in the cold-tongue can also be seen to be  
440 mainly dominated by the effects of horizontal (warming) advection, although the vertical and  
441 horizontal components do switch roles in the later warming stages in the latitudes between  
442  $140^{\circ}\text{W}$  and  $110^{\circ}\text{W}$ . This eastern-Pacific patch of warm SSTA later diminishes in amplitude due  
443 to the effects of horizontal (cooling) circulation changes. Examining the model current  
444 anomalies, we have confirmed that the horizontal advection anomalies discussed above are  
445 driven mainly by changes in the zonal, rather than meridional component (not shown for  
446 brevity).

447 The same type of diagnostic-analysis has been performed on a model experiment in which a  
448 composite MJO wind stress anomaly, based just on MJO events that contain a C-type WWE, was  
449 used to drive the model. In this case, an initial June/July cooling is seen in the eastern-Pacific  
450 (approx.  $140^{\circ}\text{W}$  to  $80^{\circ}\text{W}$ ) due to the presence of the MJO-related surface easterlies in the  
451 applied wind composite. Following this initial cooling, however, the diagnostic results (Fig. 9)  
452 reveal that the ocean processes that create warm upper ocean temperatures following this MJO+  
453 C-type WWE wind anomaly are similar in character to those that cause the warming in the C-  
454 type WWE case discussed above. Here again, the cold-tongue warming that is seen 2-3 months  
455 after the application of the wind anomaly is mainly driven by anomalous horizontal temperature  
456 advection. It may be noted, however, that in this case the vertical advection component also

457 contributes to some of the later warming seen in the 140°W-110°W longitude band (with  
458 horizontal advection in this case reversing from its otherwise warming-tendency).

459 Cold tongue warming like that seen following a WWE or MJO+WWE is not seen following the  
460 application of the composite MJO wind anomaly that is based on just the events that do not  
461 contain an embedded WWE (Fig. 10). As in the two experiments discussed above, however, the  
462 temperature changes that are seen in this case are still initiated and mainly driven by wind-driven  
463 changes in horizontal advection.

464 In summary, it is mainly the wind-driven changes in the horizontal (zonal) ocean heat flux  
465 divergence that is responsible for the equatorial warming that is seen in the model following the  
466 application of WWE-related wind anomalies. It should be recognized, however, that the  
467 equatorial warming that occurs in the model results from a small imbalance between two large  
468 (horizontal heating + vertical cooling) components.

## 469 **7. Distribution of MJO-events and WWEs**

470 In this section we more closely examine the relationship between the timing of the MJO and  
471 WWEs, focusing mainly, but not exclusively, on the events occurring in ENSO-neutral  
472 conditions. Our intent is to determine whether the historical record supports WWEs being  
473 considered characteristic of – perhaps implying a causal relationship with - the MJO, as has  
474 previously been suggested (e.g. Seiki and Takayabu, 2007), or whether it is best to think of  
475 WWEs and MJO-events as distinctly distributed events. To do this we determine the numbers of  
476 MJO events that do and do not contain a WWE, as well as the numbers of WWEs that occur and  
477 do not occur during an MJO event. The historical distributions of events will be compared to  
478 those produced in a Monte Carlo simulation that randomly distributes the same number of events

479 throughout the period(s) considered to identify any characteristics of the observed distributions  
480 that cannot be easily explained by the effects of random selection and therefore could be  
481 suggestive of a causal relationship.

482

483 The respective categories of MJO and WWEs are defined as follows. An MJO event that  
484 contains a WWE is one in which the start-day of at least one W-, C- or E-type WWE occurs  
485 during it. The remaining MJO events do not contain a WWE. As described in the methods  
486 section, WWEs are defined as days in which the defining-region average wind speed anomaly is  
487  $> 2$  m/s for at least 3 consecutive days, with the WWE start-day being the first of these days. A  
488 WWE that occurs during an MJO-event is one in which the start-day occurs during one of the  
489 identified MJO events. The remaining WWEs do not occur during an MJO event.

490 For each ENSO-condition considered, there are some MJO events that do and some that do not  
491 contain a WWE, but not in equal numbers (Table 2). Over all ENSO-conditions, the number of  
492 MJO events with a WWE exceeds the number that do not contain a WWE, but what does this  
493 result say about whether or not the chance of seeing a WWE is affected by the state of the MJO?  
494 To decide this properly, the characteristic duration and frequency of the MJO, as well as  
495 frequency of WWEs must be taken into account.

496

497 In ENSO-neutral conditions there were 62 MJO events identified, including 42 that contain a  
498 WWE and 20 that do not. The average duration of these MJO events is 34 days, with the  
499 shortest lasting 20 days (one of our event-criteria), and the longest being a rather impressive  
500 sequence of 153 days in which phases 1-8 were cycled-through three times. Based on the

501 definitions used here, the MJO was in “event-state” 40% of the time that the NIÑO3 index had  
502 magnitude  $< 0.75^{\circ}\text{C}$  in the 1986-2010 period. During this same time there were 256 WWEs  
503 identified with start-days in ENSO-neutral conditions. We performed bootstrap-Monte Carlo  
504 simulations ( $N=10000$ ) to test whether the observed fraction of MJO events with/without a  
505 WWE is unusual compared to those expected based on a purely random scattering of this number  
506 of WWEs about the identified time-history of MJO activity. The average value, 5%- and 95%-  
507 confidence levels from the Monte Carlo simulations are shown in Figure 11, where it can be seen  
508 that the observed number of MJO events that contain a WWE (42) is very close to the most  
509 likely value (43 - to the nearest whole number), and well within the 5% (37) and 95% (48)  
510 confidence levels. It follows that the observed number of MJO events that do not contain a  
511 WWE also fits easily within the simulated (random) distribution. Thus, the null-hypothesis, that  
512 WWE-likelihood remains the same whether or not an MJO-event occurs, holds for ENSO-  
513 neutral conditions.

514

515 It is evident from the values in Table 2 that the fraction of MJO events with a WWE greatly  
516 increases moving from ENSO-neutral to warm-ENSO conditions, during which time 25 out of 26  
517 MJO were observed to contain a WWE. It came initially at some surprise to the authors to find  
518 that results from the same type of Monte Carlo simulation as described above, except applied to  
519 the warm-ENSO ( $\text{NIÑO3} > 0.75^{\circ}\text{C}$ ) portion of the record, show that even this result is not  
520 statistically significant; that is, not much different than should be expected based on random  
521 selection of WWE start-times. This can be understood by considering that although the fractions  
522 of time that the MJO is in “event-state” in both ENSO-neutral and –warm conditions are about  
523 the same, the frequency of WWEs increases substantially moving from neutral to warm-ENSO

524 conditions. Specifically, the WWE frequency increases from  $\sim 1.3$  per month (256 WWEs in  
525 5784 days) in ENSO-neutral, to  $\sim 2.4$  per month (136 WWEs in 1744 days) in warm-ENSO  
526 conditions. This increase in WWE frequency as the ENSO SSTAs warm is consistent with the  
527 findings of Harrison and Vecchi (1997) and Vecchi and Harrison (2000), which were based on a  
528 substantially shorter record, along with the many other aforementioned studies (e.g. Lengaigne *et*  
529 *al.* 2004; Vecchi *et al.* 2006; Eisenman *et al.* 2005; Gebbie *et al.* 2007; Gebbie and Tziperman,  
530 2009.a,b) that have examined the dependence of WWE frequency on ENSO-state. Due to the  
531 relatively high frequency of WWEs in warm-ENSO conditions, it simply becomes rather  
532 difficult to randomly choose an MJO-event-sized time-span that does not contain at least 1 WWE  
533 in warm ENSO-conditions. The most common Monte-Carlo result in this case was finding that  
534 23 of the 26 MJO events contained at least one randomly-scattered WWE. Although the  
535 observed number (25) is slightly larger, it is not statistically significant at standard ( $p > 0.8$ )  
536 confidence levels.

537

538 As a point of comparison, it is notable that results comparable to Seiki and Takayabu's (2007)  
539 finding, based on different MJO and WWE definitions than used here, that the fraction of MJO  
540 events that contain WWEs tends to increase with MJO amplitude (c.f. their Figure 14) can also  
541 be seen in the distribution of events discussed here. When the 62 ENSO-neutral MJO events we  
542 identify are ranked based on the maximum daily MJO-amplitude attained during the event, for  
543 example, it is revealed that 9 of the top 10, and all 5 of the top 5-ranked MJO-events contain  
544 WWEs. Before imputing meaning to this result, however, it is important to test the null  
545 hypothesis that such a result can easily be explained by chance. In this case, Monte Carlo results  
546 again show that it can. It bears noting that another characteristic of MJOs that increases with



547 amplitude is their length; there is about a factor of 2 difference between the average lengths of all  
548 62 MJO events (33 days) and the top-ranked events (61 and 78 days in the top-10 and top-5  
549 cases, respectively). It is simply difficult to randomly choose such (longer-than-average) lengths  
550 of time without bracketing at least one of the 256 WWEs observed in the period considered. In  
551 each case (top-5 and top-10), there was a better than 50% chance that the number of MJO-with-  
552 WWE events found by the Monte Carlo model met or exceeded the numbers (9/10, and 5/5) seen  
553 in the observed record. Thus, this is not a statistically significant relationship. Our results  
554 therefore do not support the Seiki et al. (2007) hypothesis that large-amplitude MJO events are  
555 especially conducive to WWEs.

556 We have also used Monte Carlo methods to examine the related question of whether the  
557 distribution of WWEs with respect to MJO-state shows any significant deviations from that  
558 expected based on chance alone. The results we find in this case are consistent with those  
559 discussed above in that both the total number of WWEs that do (92) and do not (164) occur  
560 during the MJO events identified in ENSO-neutral conditions (Fig. 12; yellow bar and inset  
561 orange bar, respectively) are not significantly different from the values expected based on  
562 random chance alone.

563 Upon closer inspection, however, we do see that when they co-occur, WWEs tend to avoid the  
564 phases of the MJO with surface easterlies in the tropical Pacific (esp. phases 1, 2 and 3) and  
565 instead frequent the later westerly phases (esp. phases 6 and 8). Although it may be at first  
566 tempting to some to draw conclusions based just on this increase in WWE-frequency in phases 6  
567 and 8, it must also be recognized that the commensurate decrease in WWE frequency during the  
568 surface easterly MJO phases means that the overall likelihood of seeing a WWE is not  
569 significantly changed by the presence of the MJO (unless the MJO is somehow able to start and

570 end in its surface westerly phase without passing through its surface easterly phases – which is  
571 not its characteristic behavior).

572 In summary, we find that when they do co-occur, there is a tendency for the WWEs to frequent  
573 the surface westerly phases of the MJO and avoid, in nearly equal numbers, the surface easterly  
574 phases of the MJO such that that the overall likelihood of seeing a WWE is not changed by the  
575 presence of the MJO, even in extreme MJO-amplitude cases. This finding is confirmed when  
576 MJO events are identified using the Maloney and Hartmann (1998) MJO definition (Figure 13).

## 577 **8. Summary and Discussion**

578 Our composites of SSTA changes observed over the last 25 years show that anomalous  
579 waveguide warming, upwards of a few tenths of a degree is seen, in an average sense, following  
580 the W- C- and E-type WWEs that occurred during ENSO-neutral conditions. Over this time,  
581 warming-anomalies with similar amplitudes and pattern are seen in the composites regardless of  
582 whether they include just WWEs that do or do not occur during an MJO event.

583 This same type of warming-anomaly is seen, in an average sense, following the  
584 contemporaneous MJO events that contain embedded WWEs, but is not seen following the MJO  
585 events that do not have embedded WWEs.

586  
587 Integration of composite WWE and MJO wind stress anomalies in a realistic primitive-equation  
588 model of the upper tropical Pacific is able to reproduce these results, in the sense that composite  
589 WWE wind stresses, and (to a lesser extent) wind stress composites from MJOs that contain  
590 WWEs drive comparable warm-SSTA anomalies in the model. However, this type of warming is  
591 not seen in the model following composite MJO-events that do not contain embedded WWEs.

592

593 Together, these results show that it is the WWE wind stress anomalies, rather than the MJO, that  
594 are important to the onset of El Niño events. This confirms the findings of Vecchi (2000), with a  
595 near doubling of period, while, on the other hand, contradicting some previous hypotheses that  
596 the MJO itself plays an important role in initiating an El Niño event. Although direct  
597 comparison between previous studies of MJO-effects on SSTA and ours is made difficult by the  
598 fact that different MJO definitions have generally been used in each case (c.f. Kessler and  
599 Kleeman 2000; Zhang and Gottshalck, 2002; Hendon et al. 2007; Seiki and Takayabu 2007;  
600 Seiki et al. 2009; Kapur et al. 2011), we suggest that the results of this study, which dissects the  
601 inter-relationships between each class of wind event and the changes in waveguide SSTA that  
602 follow them, nonetheless provide a generally useful perspective from which to better understand  
603 the seemingly disparate claims about WWE and MJO effects that exist in the published  
604 literature.

605 The co-occurrence of MJO and westerly wind events, as defined here, is common enough that it  
606 is not difficult to find MJO events with embedded WWEs regardless of the definitions used, and  
607 it is evident that waveguide warming, like that which follows solo-WWEs, will often be seen  
608 following the MJO events that contain a WWE. Further, it is reasonable to expect that different  
609 MJO definitions will capture relatively more or less of the effects of these WWEs, but the results  
610 discussed here strongly suggest that even the most skillful prediction of the state of the MJO will  
611 not be useful in predicting the development of El Niño events since the MJO does not itself  
612 contribute to waveguide warming, nor does it affect the net chances, even in the case of extreme-  
613 amplitude MJO events, of seeing a WWE.

614 On the other hand, our results are consistent with (though do not explain) previous findings that  
615 WWE frequency increases with the transition from ENSO-neutral to warm-ENSO conditions,  
616 thereby increasing the influence of WWEs on ENSO (Harrison and Vecchi 1997; Vecchi and  
617 Harrison 2000; Lengaigne *et al.* 2004; Eisenman *et al.* 2005; Vecchi *et al.* 2006; Gebbie *et al.*  
618 2007; Gebbie and Tziperman, 2009.a,b; Harrison and Chiodi, 2009). That is, although WWEs  
619 are high frequency and the details of each event have a substantial stochastic component, the  
620 strong relationship between WWE frequency and ENSO-state makes WWEs, to a large degree,  
621 an element of the “slow” coupled ocean-atmosphere processes that help drive and maintain  
622 equatorial Pacific waveguide warming during El Niño events. WWEs are not best thought of as  
623 external “additive” noise.

624 Thus, forming a better understanding of the sources and predictability of WWEs remains an  
625 avenue improving our understanding of the mechanisms for initiation, and potential  
626 predictability of an El Niño event, but it does not seem that effort to better understand the MJO,  
627 though potentially quite useful in many other important respects, will provide this.

628

629

630

631

## 632 **Appendix A: MJO and WWE composite wind anomalies**

633

634 Figure A1, herein, shows the composite wind anomalies for each phase of the MJO. In this case  
635 the composites are averages of the daily wind anomalies for each day that the MJO amplitude

636 was  $> 1$  and the MJO was in the given phase. Only ENSO-neutral days are considered in this  
637 case.

638 Figure A2 shows the Day 0 composite wind anomalies for the W-, C- and E- type WWEs that  
639 occurred in ENSO-neutral conditions in the 1986-2010 period. In each case, the anomalies with  
640 statistically significant zonal components are marked by bold vectors.

## 641 **Appendix B: Monte Carlo methods**

642 This appendix describes the methods used for determining whether or not the anomaly  
643 magnitudes seen in the composites of observed variables (e.g. SSTA-changes following the MJO  
644 and WWEs, event composite wind anomalies) can easily be obtained by random selection of  
645 dates, or instead, whether they are statistically significant. This process is conceptually  
646 straightforward in that the compositing procedure used for the observations is simply repeated in  
647 the Monte Carlo simulation, except that in the Monte Carlo case, the composited days are chosen  
648 randomly. Specifically, a number of days are randomly chosen from the distribution of days  
649 considered (e.g. all those in which  $|\text{Niño3}| < 0.75^\circ\text{C}$ ) and averaged, repeatedly, to build up a  
650 distribution of possible outcomes, to which the observed result is compared. If the observed  
651 result lies at the narrow tail of this distribution (e.g.  $p > 0.95$ ) then it is considered statistically  
652 significant. If the likelihood of getting the observed result by chance is higher than this, they are  
653 not.

654 In such statistical methods it is often important that the number of effectively independent  
655 samples contained in the actual and bootstrap-composites be consistent with one another.

656 Traditionally, the number of “degrees of freedom” in the actual composite has been determined  
657 as a function of the sample autocorrelation (ACF) function (e.g. Leith 1973). Here, we use a

658 procedure that yields results consistent with the traditional methods, but avoids the burden of  
659 calculating the ACF at each grid point considered. Instead, we rely on the observed frequency of  
660 events to reproduce the effects of any observations that may lie within an “effective time  
661 between independent samples”. To do this we begin at a random date within the subset of dates  
662 considered, and then select samples from the (modulo) historical record, with sample-to-sample  
663 time lags randomly chosen from the observed time-lags that lie within the continuous ENSO-  
664 neutral periods, until the bootstrap and observed SSTA-change composites contain the same  
665 number of samples. In this way, the average effects of closely-spaced observations, that is,  
666 observations that occur too close together in time to be considered independent of one another, is  
667 reproduced in the bootstrap procedure in a manner consistent with the observations. We chose  
668 this method since it alleviates the computationally intensive need to determine autocorrelation  
669 characteristics for each of the (spatially varying) fields considered. Trial has shown that the  
670 difference between including and not including these effects of closely-spaced observations on  
671 the estimated confidence intervals, though not negligible, can be neglected without  
672 fundamentally changing the results discussed here (i.e. the timings of the WWEs and MJO-  
673 events are such that each can almost be considered to be associated with an independent sample  
674 of the target variable).

## 675 Appendix C

676 The figure herein shows the results of applying an idealized MJO composite wind stress anomaly  
677 to the ocean model. The results in this figure were obtained by the same experimental  
678 procedure used to produce the results shown in Figure 5, except in this case the specified MJO  
679 phase-duration varies according to the average duration observed in the identified MJO events,  
680 which ranges from 3 to 5.5 days and is 4.5 days, on average.

681 **Acknowledgements:**

682 *This publication is [partially] funded by the Joint Institute for the Study of the Atmosphere and Ocean*  
683 *(JISAO) under NOAA Cooperative Agreement NA10OAR4320148, Contribution No.2021 and by support*  
684 *from the Climate Observations Division of the NOAA Climate Program Office as well as from NOAA's*  
685 *Pacific Marine Environmental Laboratory. This is also NOAA PMEL contribution number 3825.*

686 **References:**

- 687
- 688 Chen, S. S., R. A. Houze, and B.E. Mapes, 1996: Multiscale variability of deep convection in  
689 relation to large-scale circulation in TOGA COARE. *J. Atmos. Sci.* **53**, 1380-1409.
- 690 Eisenman, I., L. Yu, and E. Tziperman, 2005: Westerly wind bursts: ENSO's tail rather than the  
691 dog? *J. Climate*, **18**, 5224–5238.
- 692 Gebbie, G. and E. Tziperman, Predictability of SST-modulated westerly wind bursts. *J. Climate*,  
693 **22**, 3894-3909.
- 694 Gebbie, G., and E. Tziperman, 2009: Incorporating a semi-stochastic model of ocean-modulated  
695 westerly wind bursts into an ENSO prediction model, *Theor. Appl. Climatol.*, **97**,  
696 doi:10.1007/s00704- 008-0069-6.
- 697 Gebbie, G., I. Eisenman, A. Wittenberg, and E. Tziperman, 2007: Modulation of Westerly Wind  
698 Bursts by Sea Surface Temperature: A Semi-Stochastic Feedback for ENSO, *J. Atmos.*  
699 *Sci.*, **64**, 3281– 3295, doi:10.1175/JAS4029.1.
- 700 Giese, B.S. and D.E. Harrison, 1990: Aspects of the Kelvin wave response to episodic wind  
701 forcing. *J. Geophys. Res.*, **95**, 7289-7312.
- 702 Giese, B.S. and D.E. Harrison, 1991: Eastern equatorial Pacific response to three composite  
703 westerly wind types. *J. Geophys. Res.*, **96**, 3239-3248.

- 704 Gnanadesikan, A. et al., (2006): GFDL's CM2 global coupled climate models - Part 2: The  
705 baseline ocean simulation, *J. Climate*, **19**(5), 675-697.
- 706 Griffies, S.M., M. J. Harrison, R. C. Pacanowski, and A. Rosati, 2003: A technical guide to  
707 MOM 4. GFDL Ocean Group Tech. Rep. 5, NOAA/Geophysical Fluid Dynamics  
708 Laboratory, Princeton, NJ, 295 pp.
- 709 Harrison, D. E., 1984: The appearance of sustained equatorial surface westerlies during the 1982  
710 Pacific warm event. *Science*, **224**, 1099-1102.
- 711 Harrison, D.E. and A.M. Chiodi, 2009: Pre- and Post-1997/98 Westerly wind events and  
712 equatorial Pacific cold tongue warming, *J. Climate*, **22**, 568-581.
- 713 Harrison, D.E., A.M. Chiodi and G.A. Vecchi, 2009: Effects of surface forcing on the seasonal  
714 cycle of the eastern equatorial Pacific, *J. Mar. Res.*, **67**, 701-729.
- 715 Harrison, D.E., and B.S. Giese (1991): Episodes of surface westerly winds as observed from  
716 islands in the western tropical Pacific. *J. Geophys. Res.*, 96(Suppl.), 3221–3237.
- 717 Harrison D.E., and G.A. Vecchi, 1997: Westerly wind events in the tropical Pacific. *J. Climate*,  
718 **10**, 3131-3156.
- 719 Hartten, L. M., 1996: Synoptic settings of westerly wind bursts. *J. Geophys. Res.*, **101**, 16997-  
720 17019.
- 721 Hendon, H.H., M.C. Wheeler and C. Zhang, 2007: Seasonal dependence of the MJO-ENSO  
722 Relationship. *J. Climate*, **20**, 531-543.
- 723 Kapur, A., C. Zhang, J. Zavala-Garay and H. Hendon, 2011: Role of stochastic forcing in ENSO  
724 in observations and a coupled GCM. *Clim. Dyn.*, DOI 10.1007/s00382-011-1070-9.
- 725 Keen, R. A., 1982: The role of cross-equatorial cyclone pairs in the Southern Oscillation. *Mon*  
726 *Wea. Rev.* **110**, 1405-1416.



- 727 Kessler WS, Kleeman R, 2000: Rectification of the Madden–Julian oscillation into the ENSO  
728 cycle. *J. Climate*, **13**, 3560–3575.
- 729 Kessler, W. S., 2001: EOF representations of the Madden–Julian oscillation and its connection  
730 with ENSO. *J. Climate*, **14**, 3055–3061.
- 731 Leith, C. E., 1973: The standard error of time-average estimates of climatic means. *J. Appl.*  
732 *Meteor.*, **12**, 1066-1069.
- 733 Lengaigne, M., J.P. Boulanger, C. Menkes, S. Masson, G. Madec, and P. Delecluse, 2002: Ocean  
734 response to the March 1997 westerly wind event. *J. Geophys. Res.*, **107**, 8015,  
735 doi:10.1029/2001JC000.
- 736 Lengaigne, M., J.-P. Boulanger, C. Menkes, G. Madec, P. Delecluse, E. Guilyardi and J. M.  
737 Slingo, 2003 : The March 1997 Westerly Wind Event and the Onset of the 1997/98 El  
738 Niño: Understanding the Role of the Atmospheric Response, *Journal of Climate*, **16**, 20,  
739 3330-3343,
- 740 Lengaigne, M., E. Guilyardi, J. P. Boulanger, C. Menkes, P. Delecluse, P. Inness, J. Cole, and J.  
741 Slingo, 2004: Triggering of El Niño by westerly wind events in a coupled general  
742 circulation model. *Climate Dyn.*, **23**, 601-620.
- 743 Lin, X., and R. H. Johnson, 1996: Kinematic and thermodynamic characteristics of the flow over  
744 the western Pacific warm pool during TOGA COARE. *J. Atmos. Sci.*, **53**, 695-715.
- 745 Love, G., 1985a: Cross-equatorial influence of winter hemisphere subtropical cold-surges. *Mon.*  
746 *Wea. Rev.*, **113**, 1487-1498.
- 747 Love, G., 1985b: Cross-equatorial interactions during tropical cyclogenesis. *Mon. Wea. Rev.*,  
748 **113**, 1499-1509.

- 749 Luther, D. S., D. E. Harrison, and R. A. Knox, 1983: Zonal winds in the central equatorial  
750 Pacific and El Niño. *Science*, **222**, 327-330.
- 751 Madden, R.A. and P.R. Julian, 1972: Description of global-scale circulation cells in the tropics  
752 with a 40-50 day period. *J. Atmos. Sci.*, **29**, 1109-1123.
- 753 Perigoud, C. M., and C. Cassou, 2000: Importance of oceanic decadal trends and westerly wind  
754 bursts for forecasting El Niño. *Geophys. Res. Lett.*, **27**, 389-392.
- 755 Philander, S.G.H. and A.D. Seigel, 1985: Simulation of El Niño of 1982-1983. In *Coupled*  
756 *Ocean-Atmosphere Models*, J. Nihoul, ed., Elsevier, 517-541.
- 757 Seiki, A. and Y.N. Takayabu, 2007: Westerly wind bursts and their relationship with  
758 intraseasonal variations and ENSO. Part I: Statistics. *Mon. Wea. Review*, **135**, 3325-  
759 3345.
- 760 Slingo, J. M., D. P. Rowell, K. R. Sperber, and F. Nortley, 1999: On the predictability of the  
761 interannual behavior of the Madden–Julian oscillation and its relationship with El Niño.  
762 *Quart. J. Roy. Meteor. Soc.*, **125**, 583–609.
- 763 Vecchi, G.A., 2000: Sub-seasonal wind variability and El Niño. Ph.D. thesis, University of  
764 Washington, 184 pp.
- 765 Vecchi, G.A., and D.E. Harrison, 2000: Tropical Pacific sea surface temperature anomalies, El  
766 Niño, and equatorial westerly wind events. *J. Climate*, **13**, 1814-1830.
- 767 Vecchi, G.A., A.T. Wittenberg and A. Rosati (2006). Reassessing the role of stochastic forcing in  
768 the 1997-8 El Niño. *Geophys. Res. Lett* 33, L01706, doi:10.1029/2005GL024738.
- 769 Wheeler, M.C. and H.H. Hendon, 2004: an all-season real-time multivariate MJO index:  
770 Development of an index for monitoring and prediction. *Mon. Wea. Rev.*, **132**, 1917-  
771 1932.

- 772 Zavala-Garay J, A.M. Moore, C.L. Perez, Kleeman R, 2003: The response of a coupled model of  
773 ENSO to observed estimates of stochastic forcing. *J Climate*, **16**, 2827–2842
- 774 Zavala-Garay J, Zhang C, Moore AM, Kleeman R, 2005: The linear response of ENSO to the  
775 Madden–Julian oscillation. *J Climate*, **18**, 2441–2459
- 776 Zavala-Garay J, C. Zhang, A.M. Moore, A.T. Wittenberg, M.J. Harrison, A. Rosati, J. Vialard,  
777 R. Kleeman, 2008: Sensitivity of hybrid ENSO models to unresolved atmospheric  
778 variability. *J Climate*. **21**, 3704–3721
- 779 Zhang, C., and J. Gottschalck, 2002: SST anomalies of ENSO and the Madden–Julian oscillation  
780 in the equatorial Pacific. *J. Climate*, **15**, 2429–2445.

781  
782 List of Figures  
783

784 Figure. 1. Composite SSTA change following the MJO events that occurred in  
785 ENSO-neutral conditions ( $|\text{NIÑO3}| < 0.75^\circ\text{C}$ ) from 1986 to 2010. Results shown  
786 separately for all 58 ENSO-neutral MJO events (left), the 17 MJO events that do  
787 not contain an embedded WWE (middle) and the 41 that do contain a WWE  
788 (right).

789 Figure. 2. Upper panels: Same as in the +80 days panels shown in Fig. 1, which  
790 are based on the Wheeler and Hendon (2004) MJO index. Lower panels: same as  
791 above, except in this case the MJO events are identified using the Maloney and  
792 Hartmann (1998) index.

793 Figure. 3. Composite SSTA-changes following W-type (left), C-type (middle) and  
794 E-type (right) WWEs that occurred in ENSO-neutral ( $|\text{NIÑO3}| < 0.75^{\circ}\text{C}$ )  
795 conditions in the 1986-2010 period.

796 Figure. 4. Composite MJO wind stress anomaly (upper panel) along with the W-  
797 type, C-type and E-type WWE composite wind stress anomalies (averaged over  
798  $2^{\circ}\text{S}$ - $2^{\circ}\text{N}$ ).

799 Figure 5. Change in model SSTA following the application of the composite MJO  
800 wind stress anomaly.

801 Figure 6. Model SSTA following the application of a composite WWE wind stress  
802 anomaly.

803 Figure 7. Model SSTA following application of a C-type WWE wind anomaly.  
804 Only WWEs that occurred in ENSO-neutral and MJO-active (-inactive) conditions  
805 were used in the composite used to drive the anomaly seen in the upper (lower)  
806 panel.

807 Figure 8. Near-surface ocean heat budget diagnostics from a C-type WWE model  
808 experiment; a) 0-50m average heat content anomaly, b) time-change in heat  
809 content anomaly expressed in  $\text{W}/\text{m}^2$ , c) sum of the heat budget terms, d) sum of  
810 just circulation-related effects, e) surface heat flux anomaly effects, f) other terms  
811 (see text). Panels (g) and (h) show the contribution of the horizontal and vertical

812 components of the circulation anomalies to the heating/cooling anomalies shown in  
813 panel (d).

814 Figure 9. Same as in Fig. 8, except for the MJO + WWE model experiment.

815 Figure 10. Same as in Fig. 8, except for the MJO-without-WWE model  
816 experiment.

817 Figure 11. Number of MJO events that do and do not contain a WWE. Period  
818 1986-2010,  $|\text{NIÑO3}| < 0.75^\circ\text{C}$ . The top, middle and lower horizontal lines about  
819 each bar show the  $p=0.95$ , expected, and  $p=0.05$  levels, respectively, based on a  
820 random distribution of events.

821 Figure 12. The numbers of WWEs that do and do not occur during an MJO event,  
822 listed by phase (based on WWE start-date) for the co-occurring case. Horizontal  
823 lines are the  $p=0.95$ , expected, and  $p=0.05$  values.

824 Figure 13. Same as in Fig. 12, except using the Maloney and Hartmann (1998)  
825 index for MJO event identification.

826 Figure A1. Composite MJO wind anomalies. Bold arrows highlight anomalies that  
827 reach the 95% confidence level based on Monte-Carlo bootstrap methods.

828 Figure A2. Westerly wind event wind anomalies.

829

830 Figure C1. Model SSTA following the application of a (variable-phase-duration)  
831 composite MJO wind stress anomaly.

832

833

834

835

836

837

838

839

840

841

842

843

844

845

## 846 Tables

847 Table 1: NIÑO3 index change 80 days following a WWE that occurs in REG-SSTA conditions.

	All WWEs (°C)	MJO-Active (°C)	MJO-Inactive (°C)
W-type	0.24	0.29	0.21
C-type	0.18	0.22	0.16
E-type	0.31	0.41	0.17

848

849

850

851 Table 2: Distribution of MJO events by ENSO-state and WWE activity.

Number of MJO events			
	Total	with WWE	No WWE
All-time	113	76	37
ENSO-neutral	62	42	20
Warm-ENSO	26	25	1

852

853

854

855

856

857

858

859

860

861

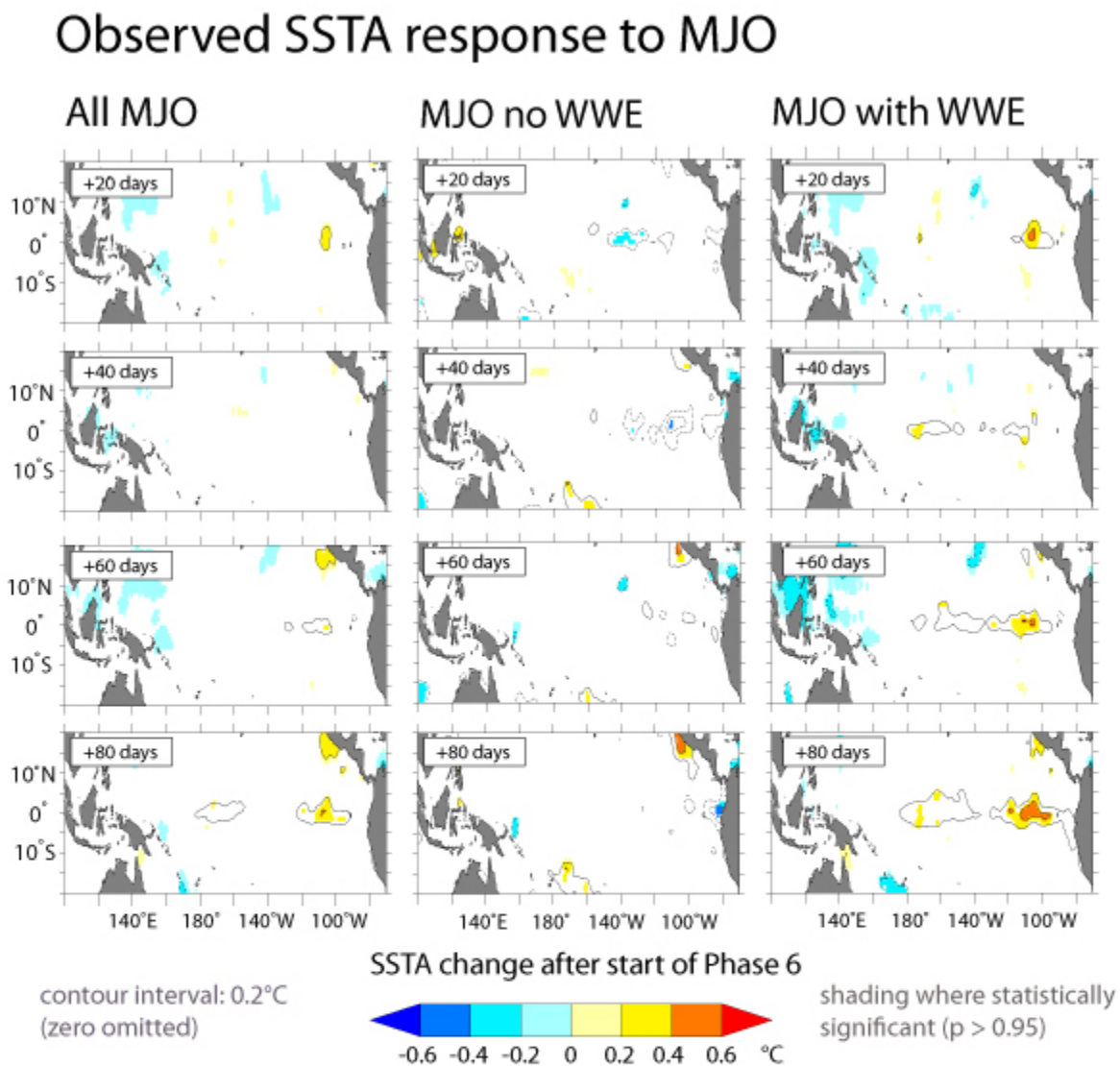
862

863

864

865

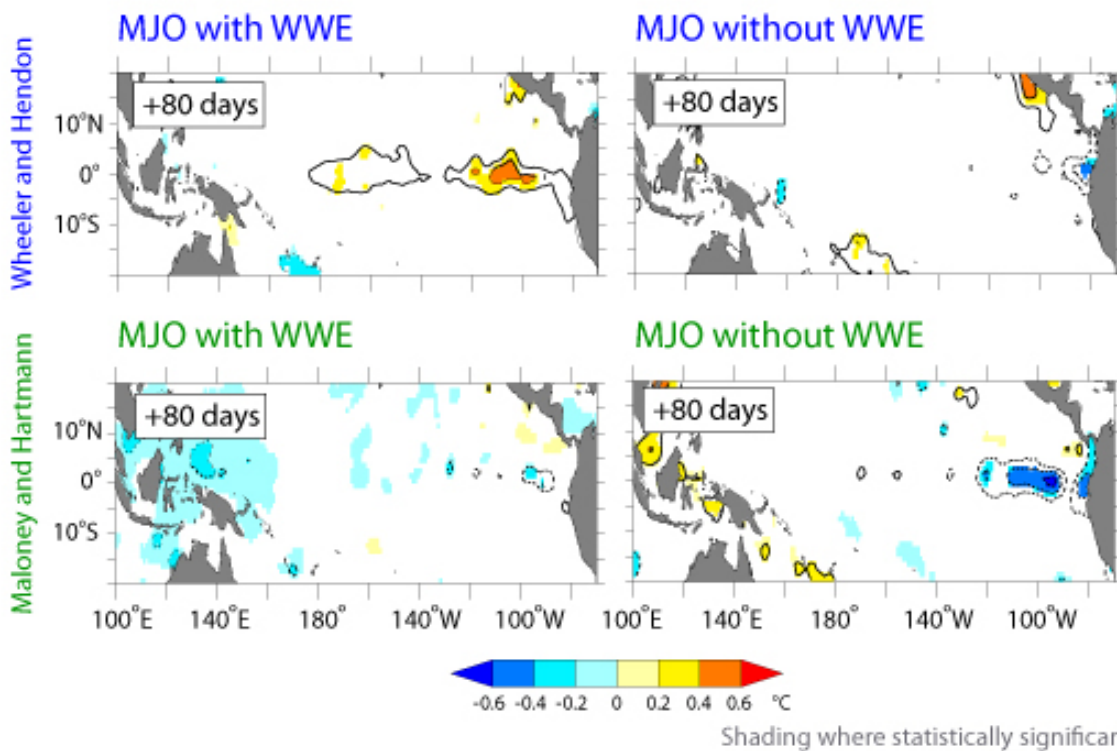
866 Figures.



867  
 868 Figure. 1. Composite SSTA change following the MJO events that occurred in ENSO-neutral  
 869 conditions ( $|\text{NI}\ddot{\text{N}}\text{O}3| < 0.75^\circ\text{C}$ ) from 1986 to 2010. Results shown separately for all 58 ENSO-  
 870 neutral MJO events (left), the 17 MJO events that do not contain an embedded WWE (middle)  
 871 and the 41 that do contain a WWE (right).



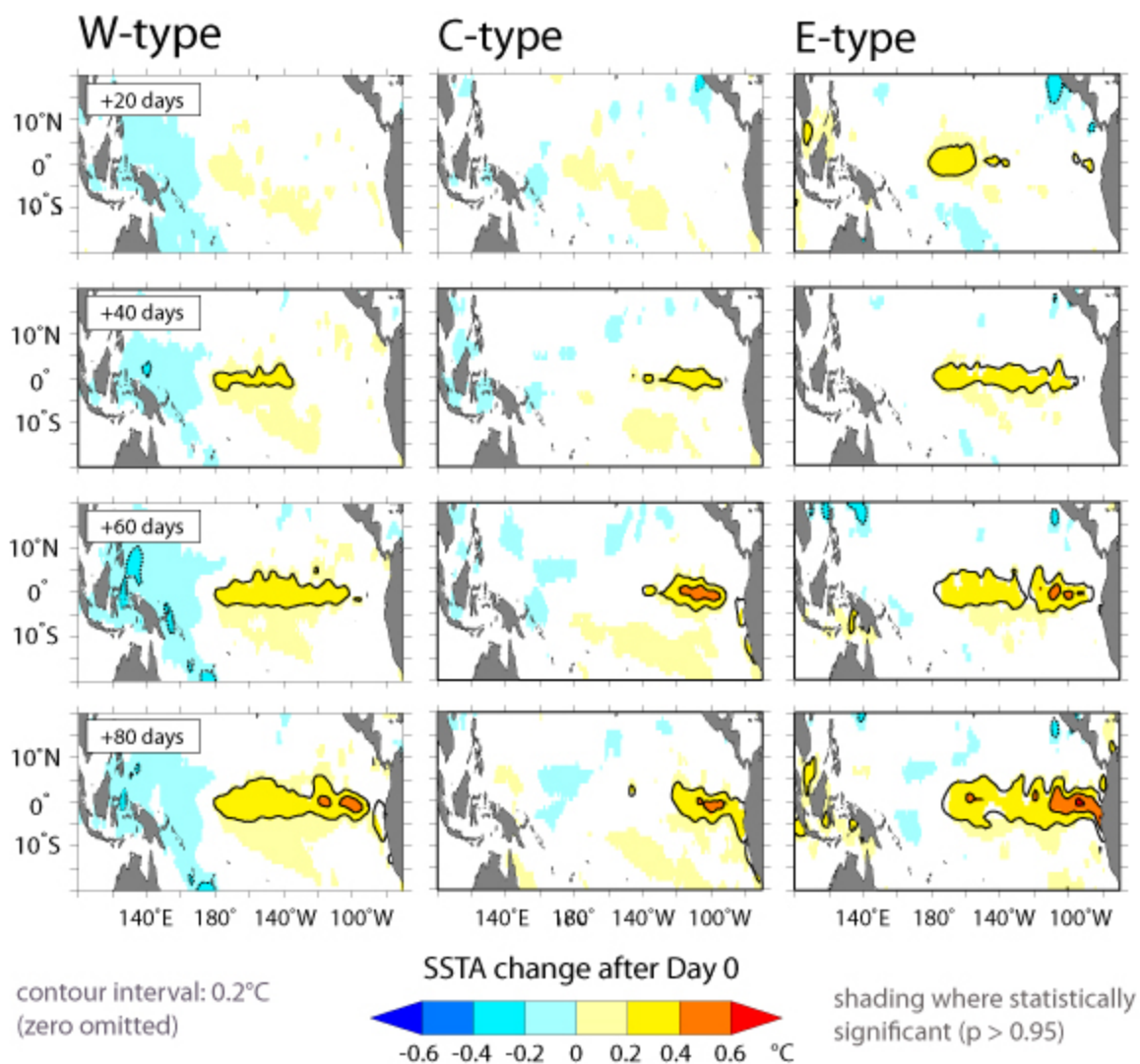
## SSTA change after start of surface-westerly MJO phase



872  
 873 Figure 2. Upper panels: Same as in the +80 days panels shown in Fig. 1, which are based on the  
 874 Wheeler and Hendon (2004) MJO index. Lower panels: same as above, except in this case the  
 875 MJO events are identified using the Maloney and Hartmann (1998) index.

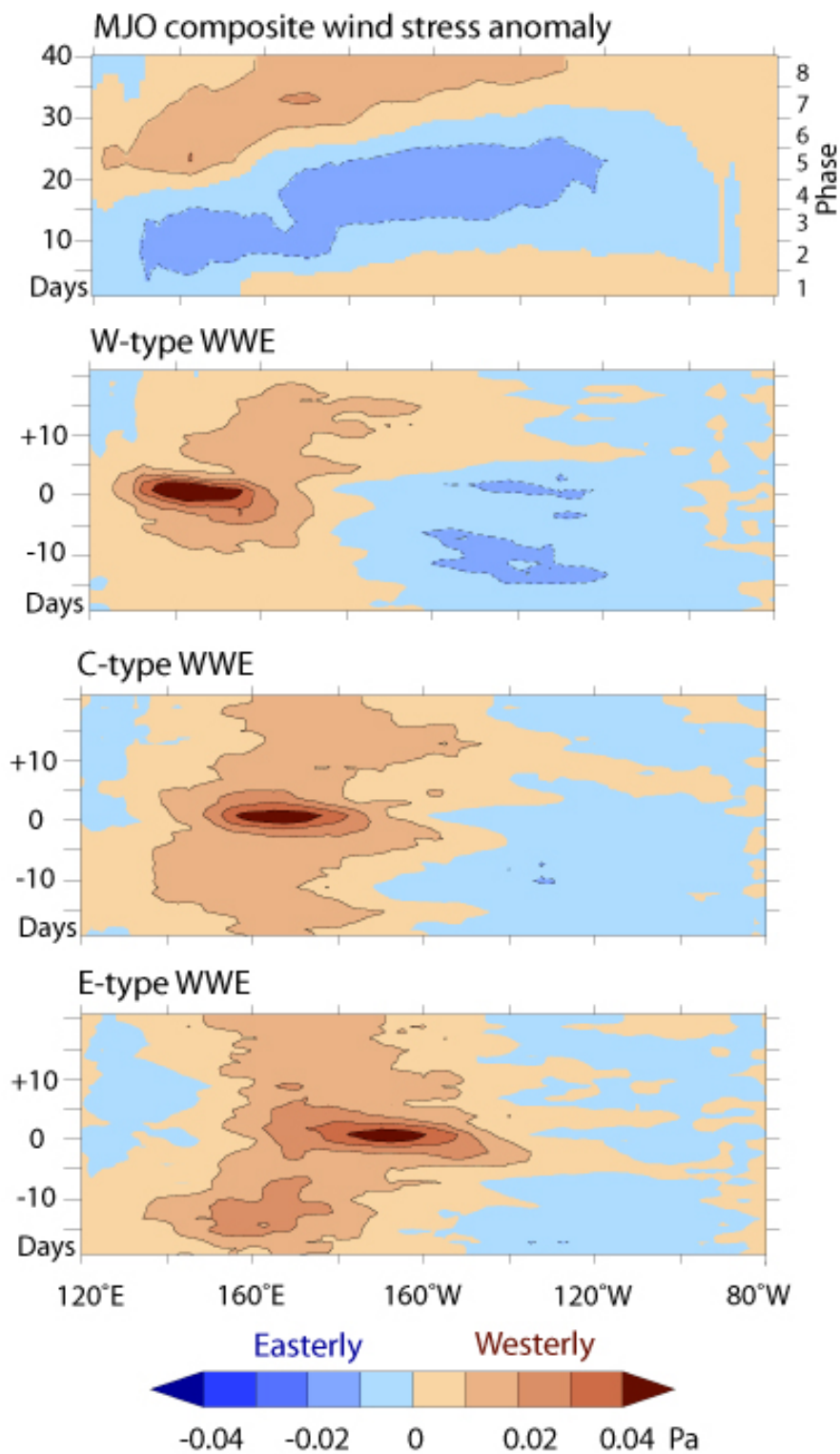
876  
 877

## Observed SSTA response to WWE



878  
879 Figure 3. Composite SSTA-changes following W-type (left), C-type (middle) and E-type (right)  
880 WWEs that occurred in ENSO-neutral ( $|\text{NIÑO3}| < 0.75^\circ\text{C}$ ) conditions in the 1986-2010 period.

881

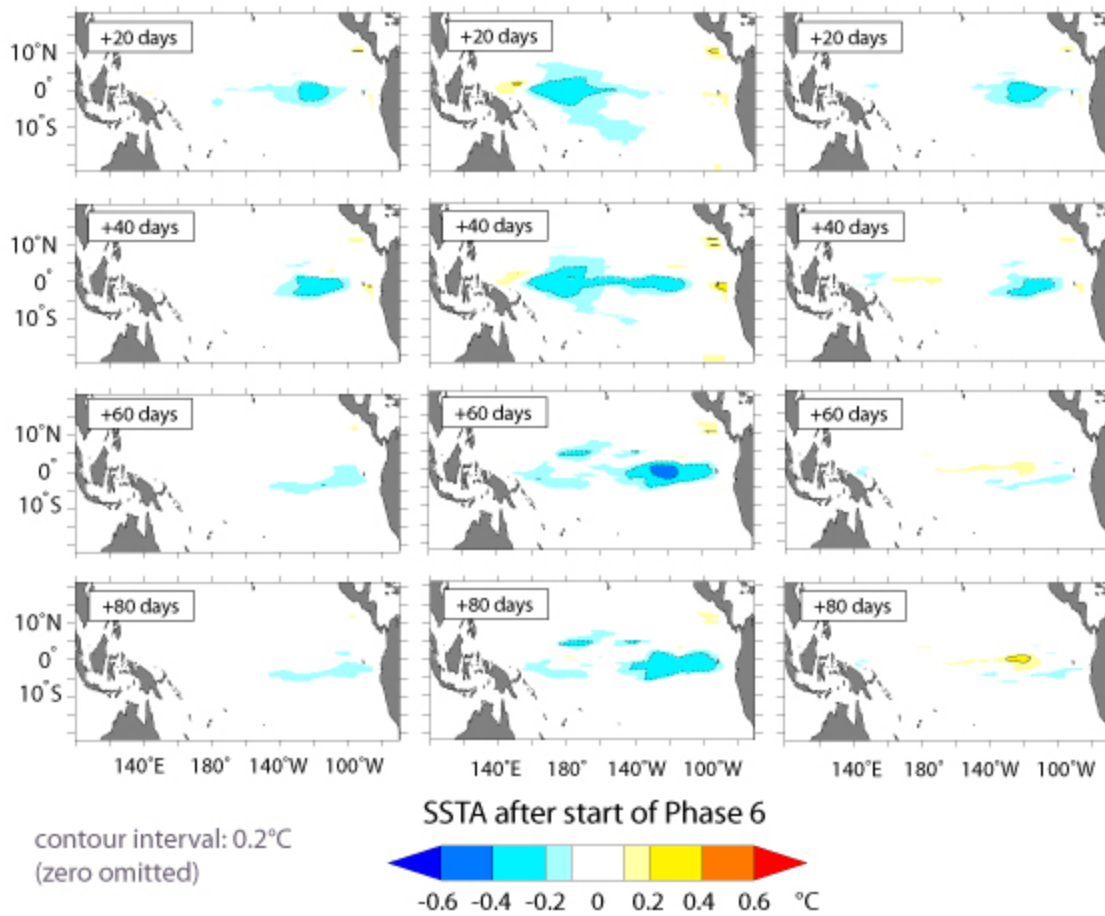


882

883 Figure 4. Composite MJO wind stress anomaly (upper panel) along with the W-type, C-type and

884 E-type WWE composite wind stress anomalies (averaged over 2°S-2°N).

## Model SSTA response to MJO



885

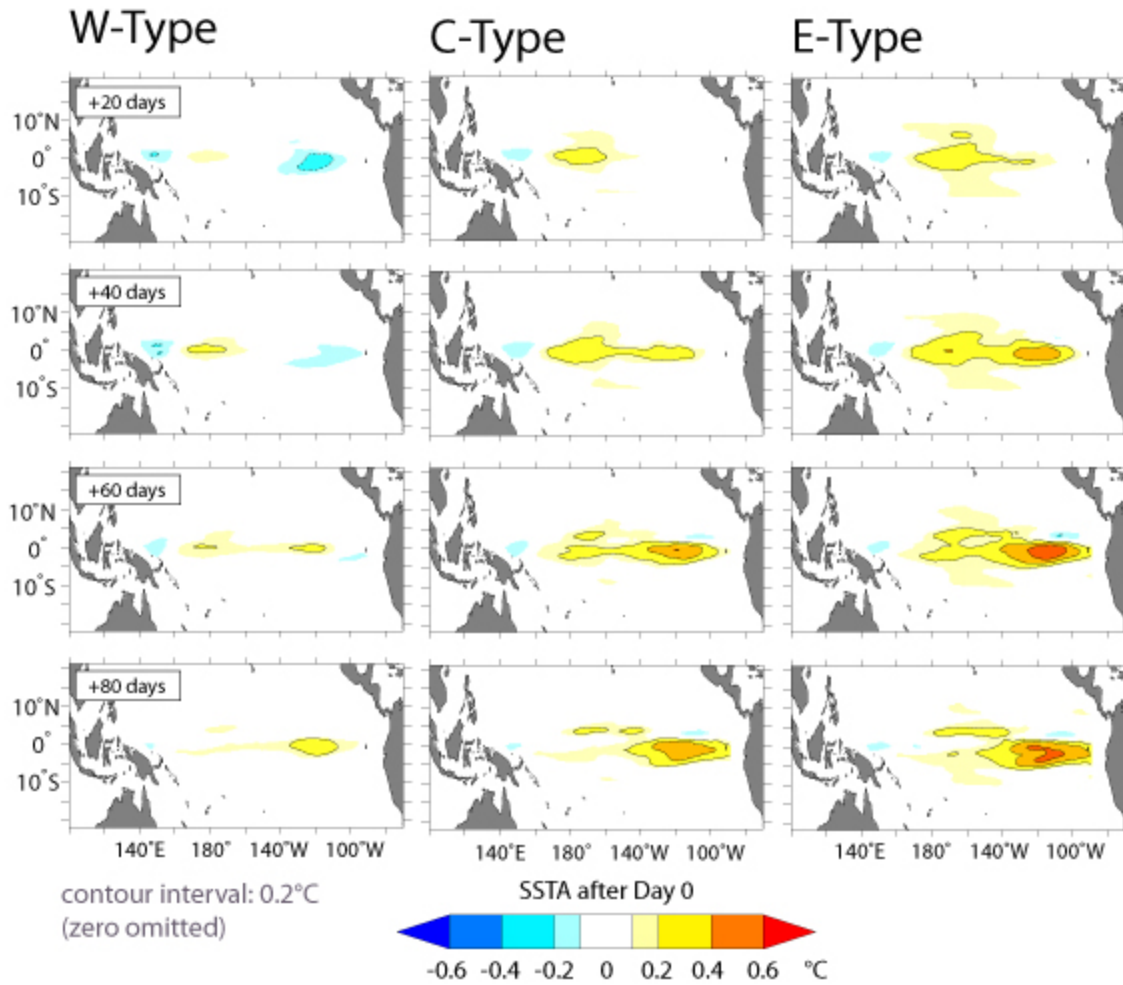
886 Figure 5. Change in model SSTA following the application of the composite MJO wind stress

887 anomaly.

888

889

## Model SSTA response to WWE



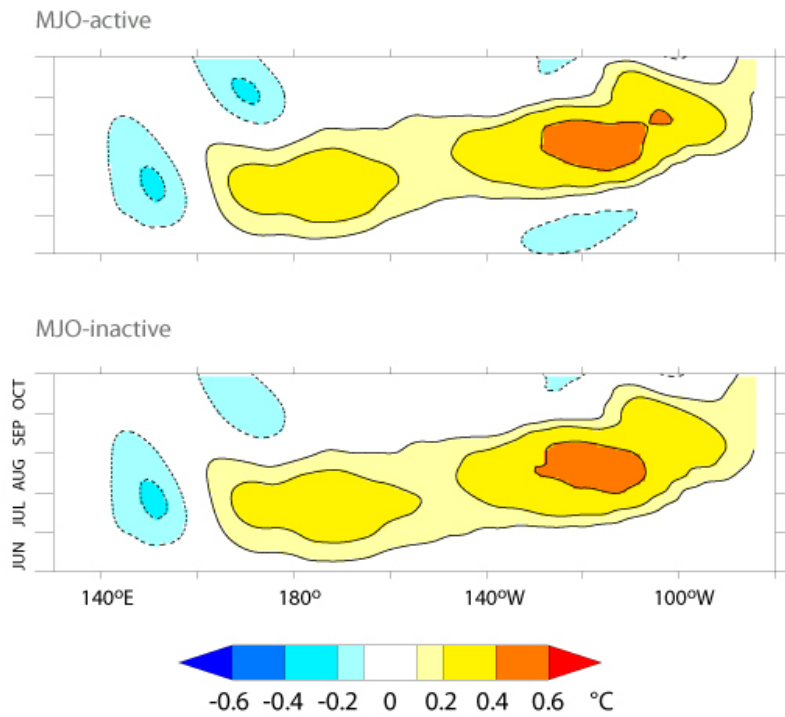
890

891 Figure 6. Model SSTA following the application of a composite WWE wind stress anomaly.

892

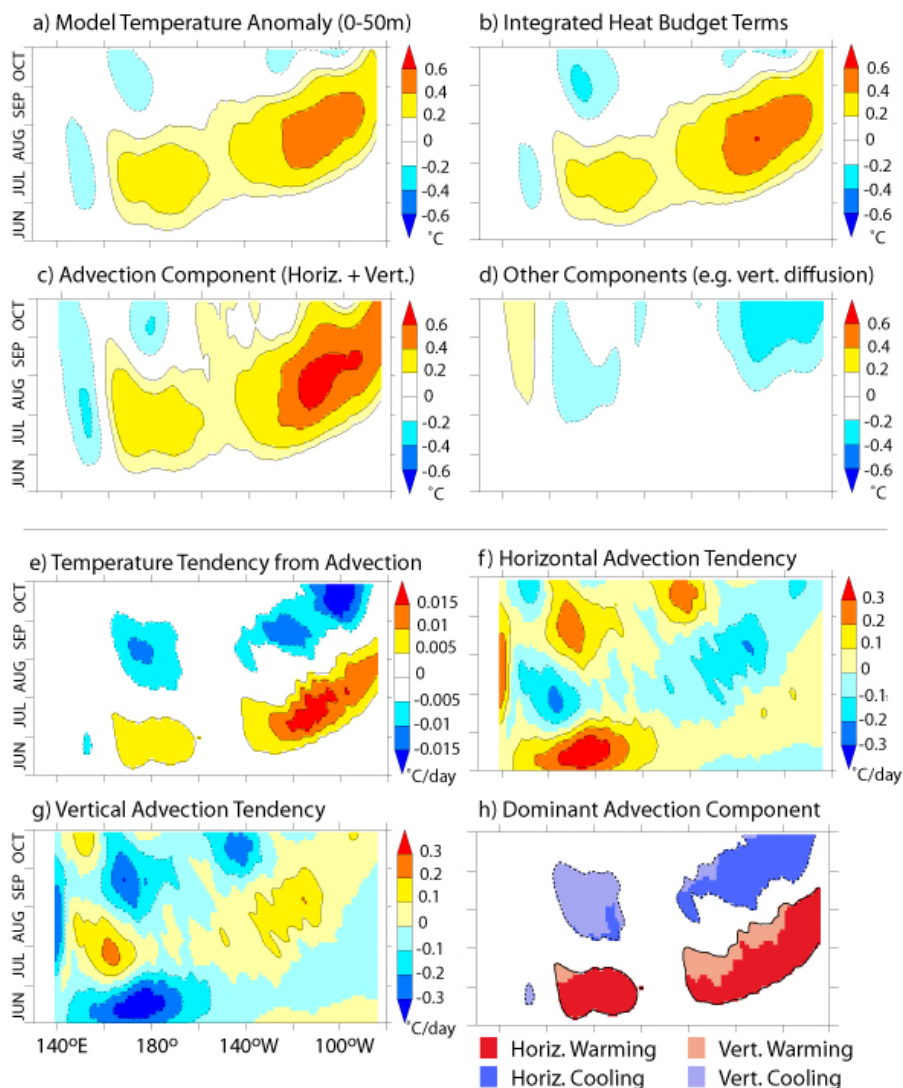
893

## Model Response to a WWE



894  
 895 Figure 7. Model SSTA following application of a C-type WWE wind anomaly. Only WWEs  
 896 that occurred in ENSO-neutral and MJO-active (-inactive) conditions were used in the composite  
 897 used to drive the anomaly seen in the upper (lower) panel.

## C-type WWE Model Run

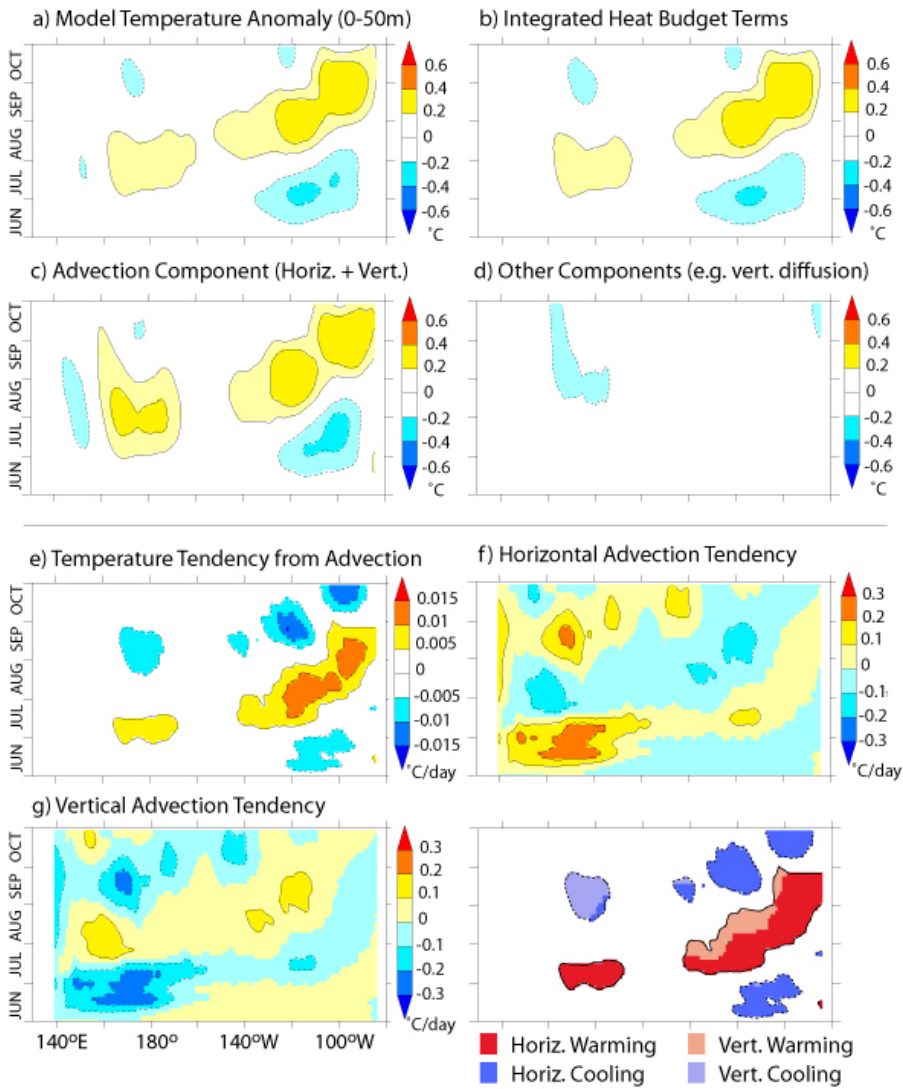


898  
 899 Figure 8. Near-surface ocean heat budget diagnostics from a C-type WWE model experiment; a)  
 900 0-50m average heat content anomaly, b) time-change in heat content anomaly expressed in  
 901  $\text{W}/\text{m}^2$ , c) sum of the heat budget terms, d) sum of just circulation-related effects, e) surface heat  
 902 flux anomaly effects, f) other terms (see text). Panels (g) and (h) show the contribution of the  
 903 horizontal and vertical components of the circulation anomalies to the heating/cooling anomalies  
 904 shown in panel (d).

905



## MJO with C-type WWE Model Run

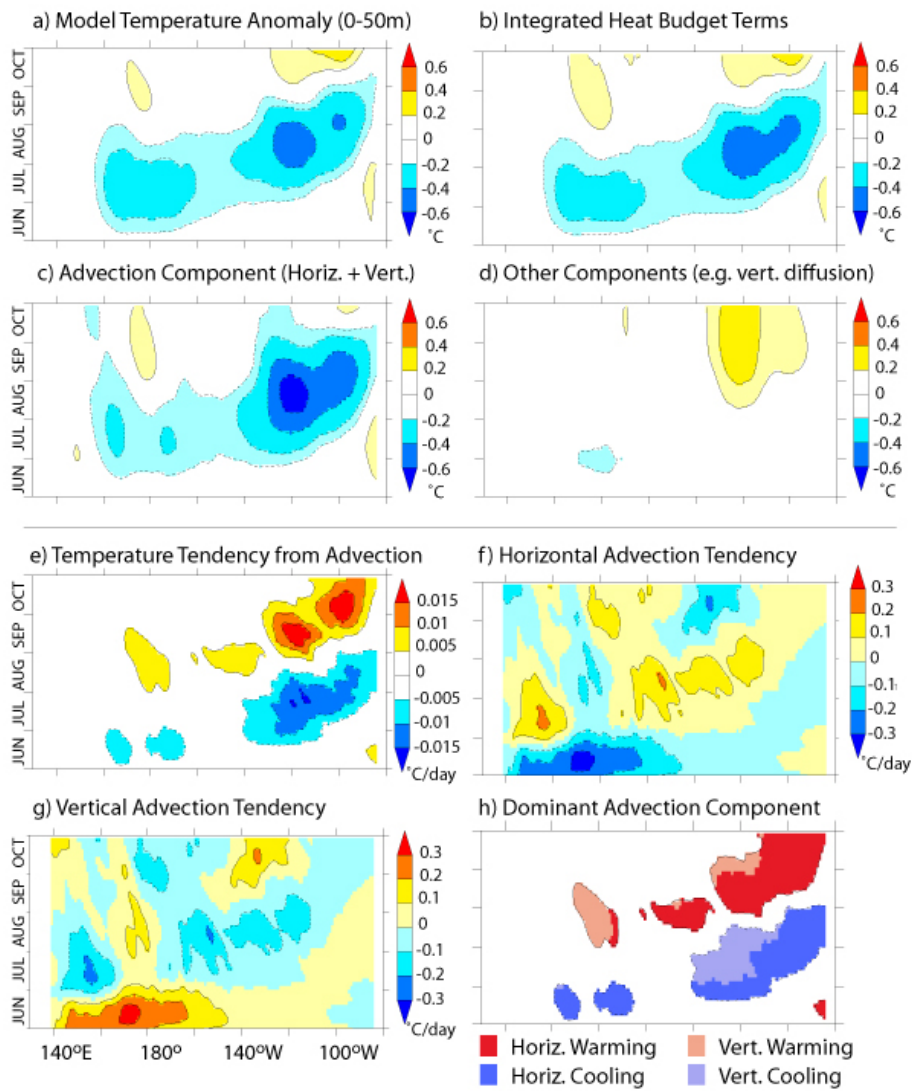


906

907 Figure 9. Same as in Fig. 8, except for the MJO + WWE model experiment.



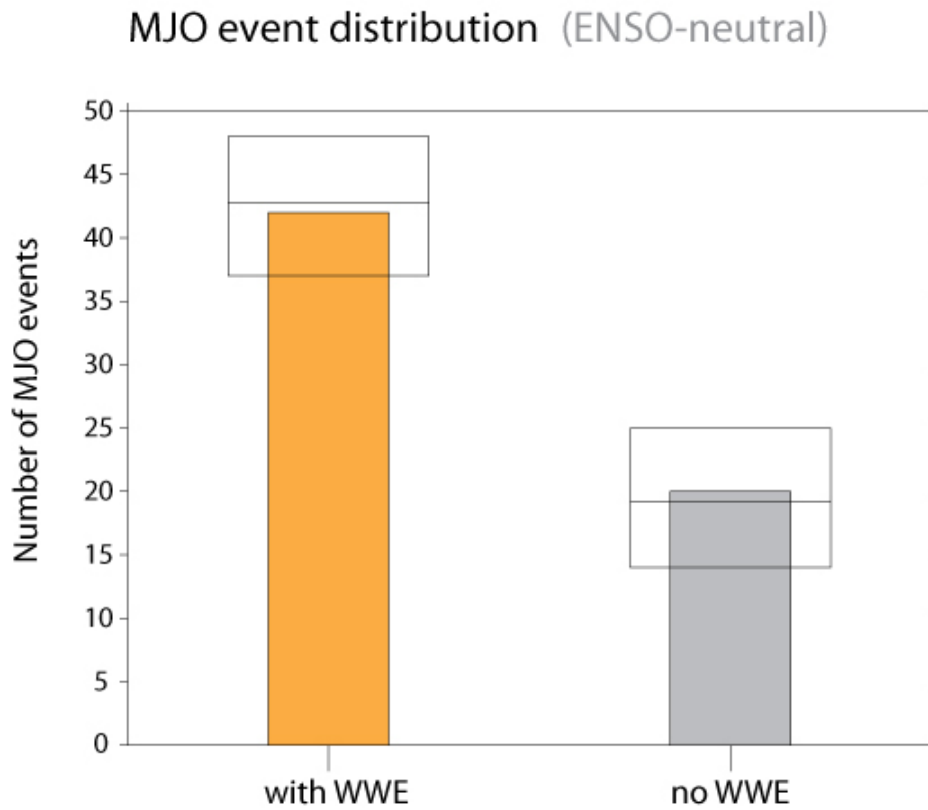
## MJO without WWE Model Run



908

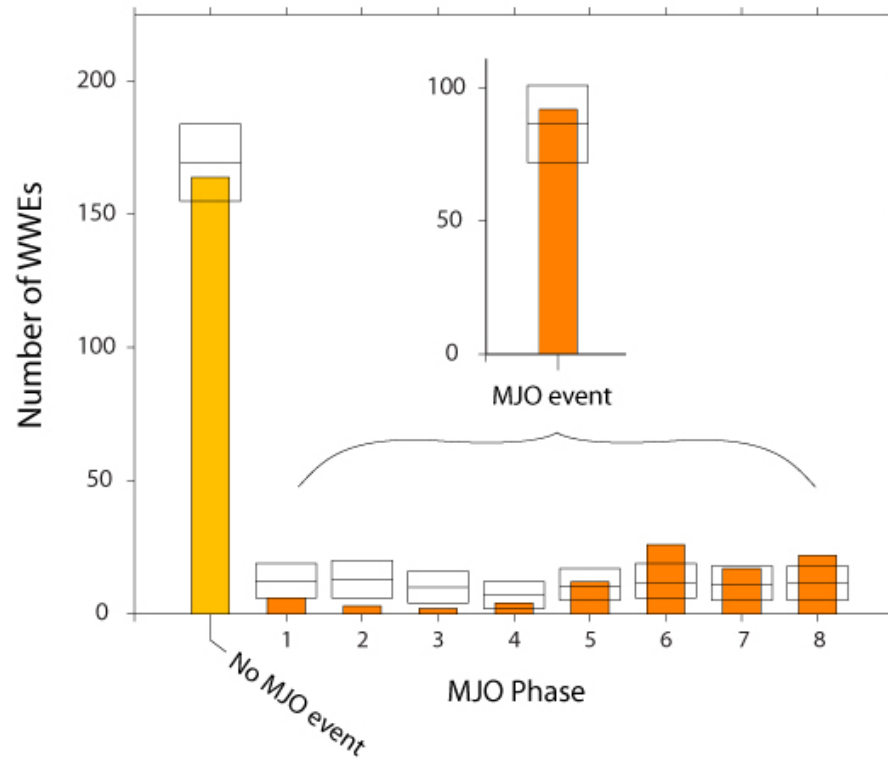
909 Figure 10. Same as in Fig. 8, except for the MJO-without-WWE model experiment.

910



911  
 912 Figure 11. Number of MJO events that do and do not contain a WWE. Period 1986-2010,  
 913  $|\text{NIÑO3}| < 0.75^\circ\text{C}$ . The top, middle and lower horizontal lines about each bar show the  $p=0.95$ ,  
 914 expected, and  $p=0.05$  levels, respectively, based on a random distribution of events.

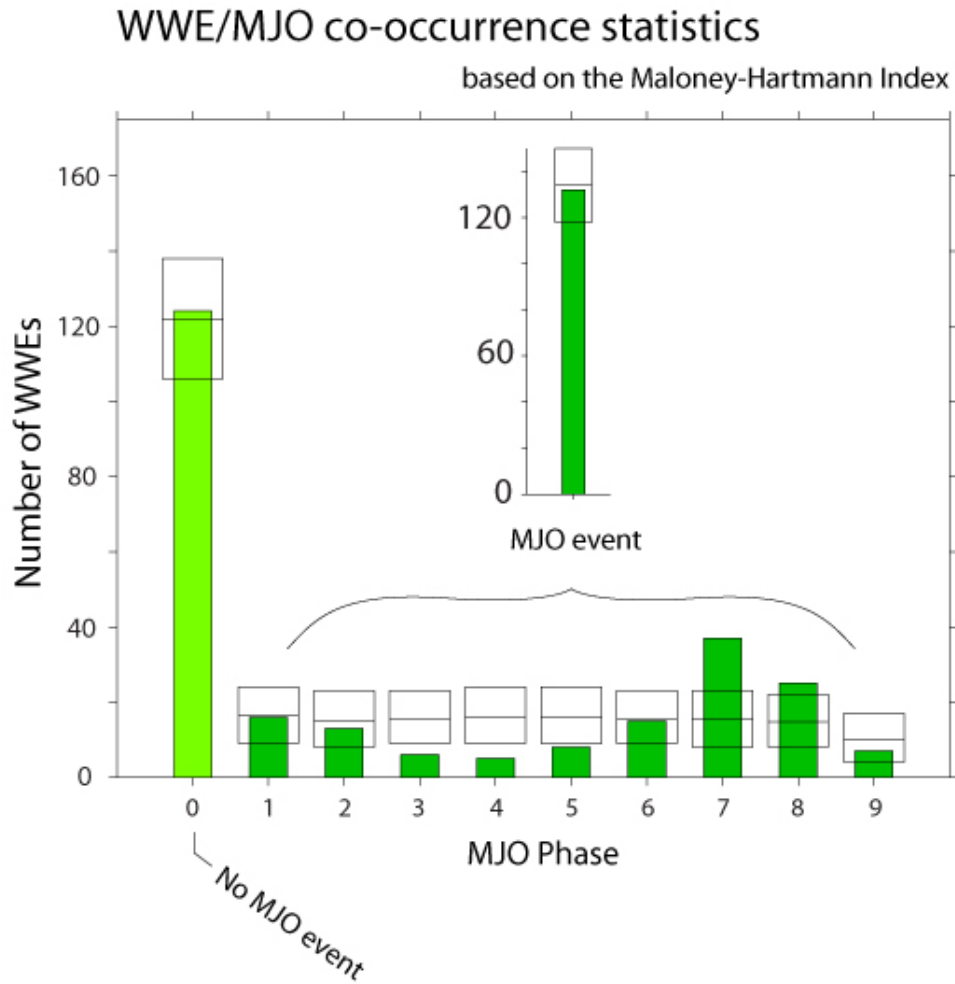
915



916

917 Figure 12. The numbers of WWEs that do and do not occur during an MJO event, listed by phase

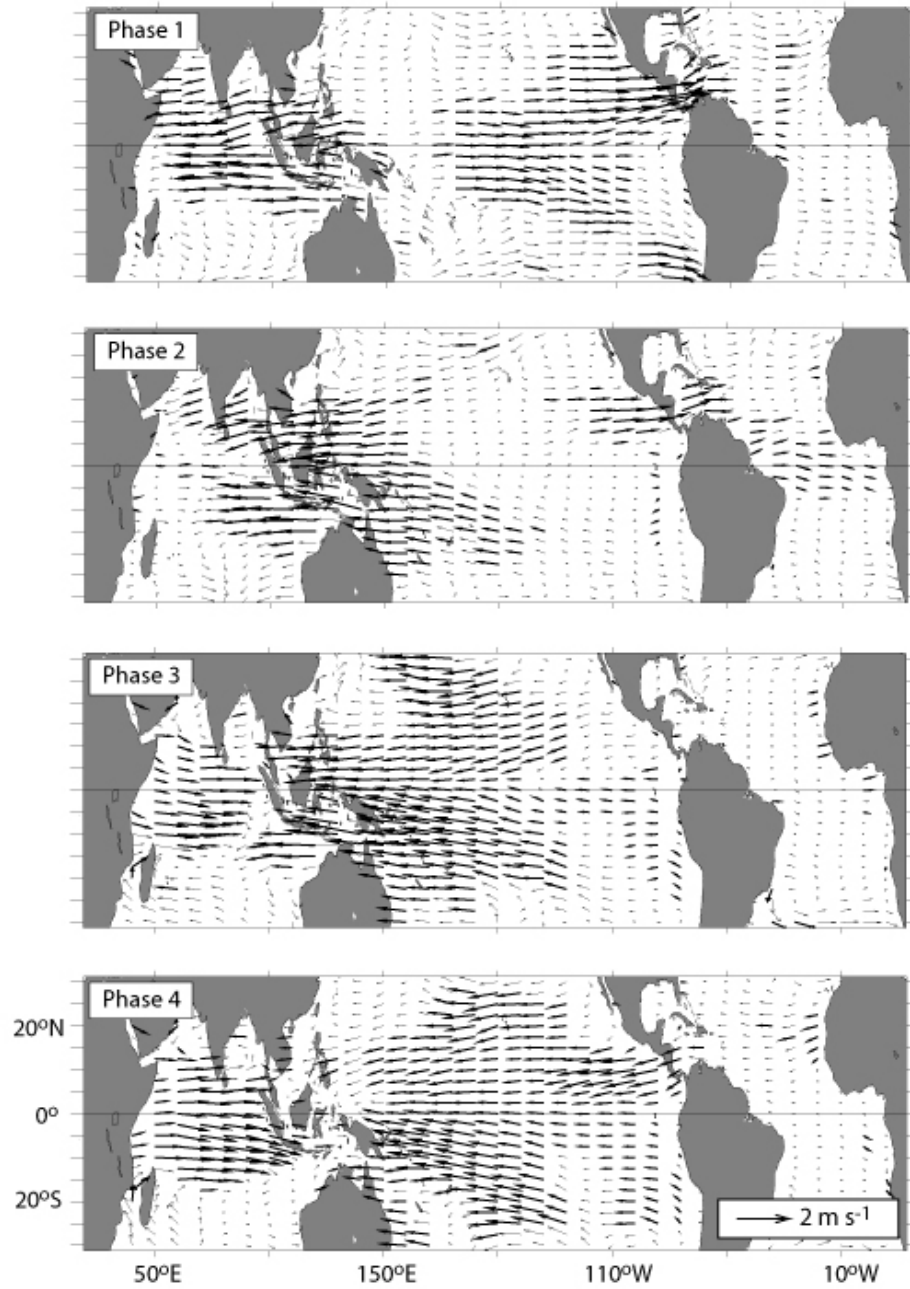
918 (based on WWE start-date) for the co-occurring case. Horizontal lines are the  $p=0.95$ , expected,919 and  $p=0.05$  values.



920

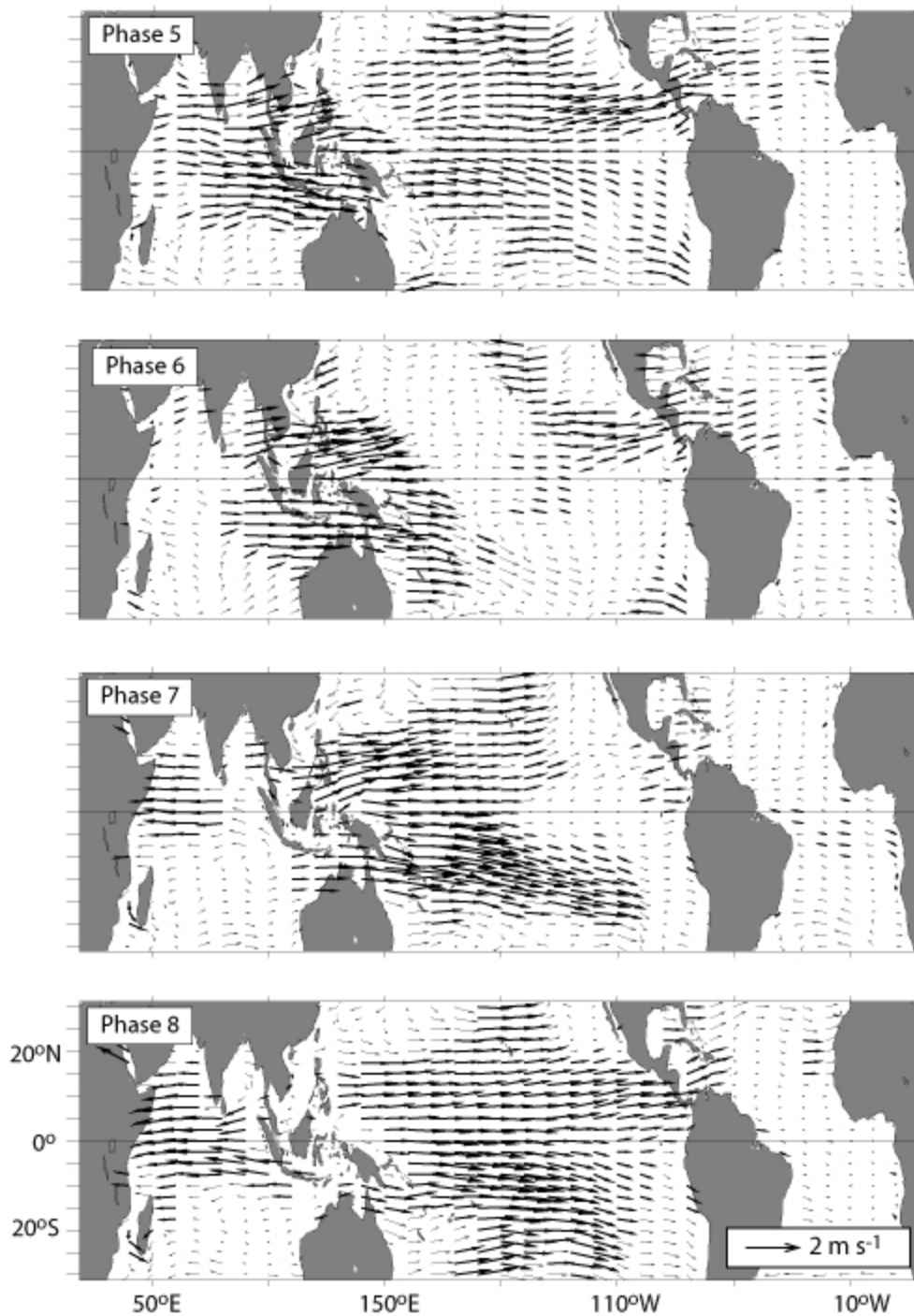
921 Figure 13. Same as in Fig. 12, except using the Maloney and Hartmann (1998) index for MJO event

922 identification.



923  
924 Fig. A1. Composite MJO wind anomalies. Bold arrows highlight anomalies that reach the 95%  
925 confidence level based on Monte-Carlo bootstrap methods.

926  
927



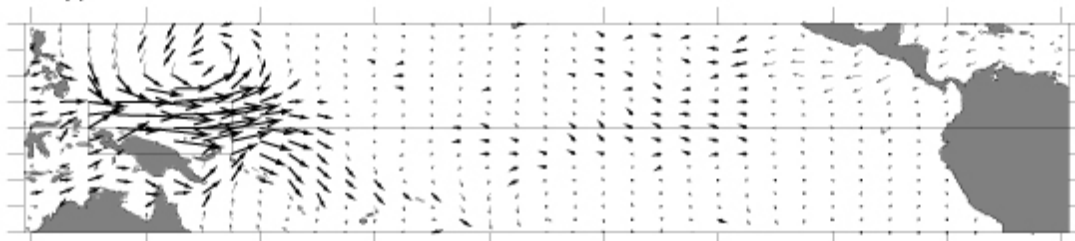
928  
929 Fig. A1 continued.  
930  
931

## WWE Wind Anomaly

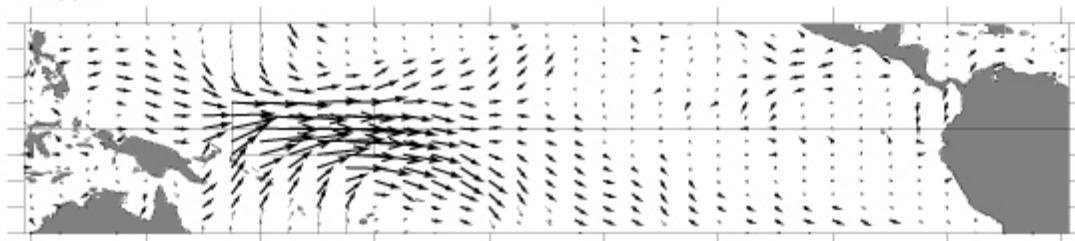
Period 1986-2010

Center-day

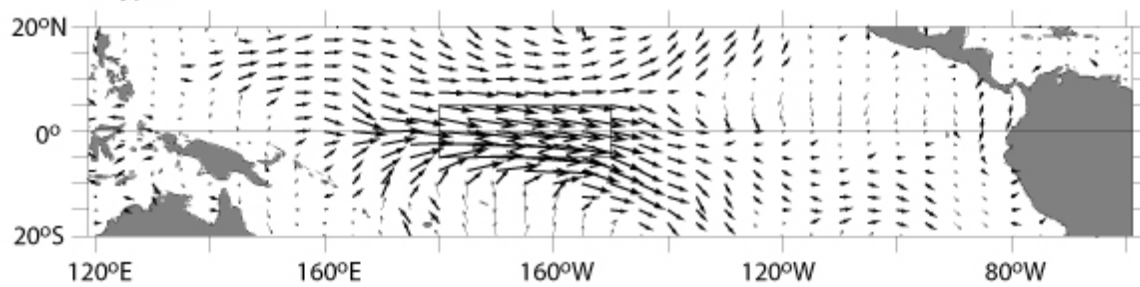
W-type



C-type



E-type

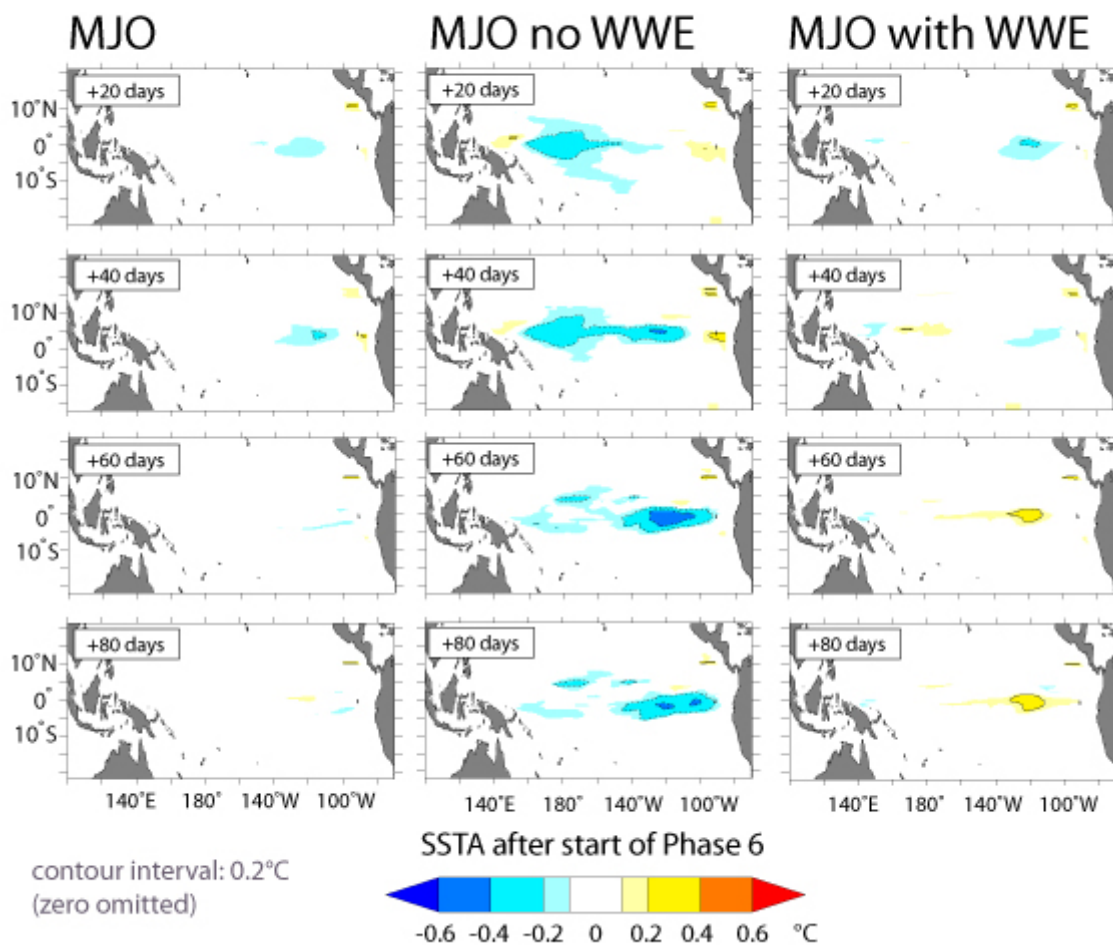


932

933 Fig. A2. Westerly wind event wind anomalies.

934

## Model SSTA response to MJO



935  
936 Fig. C1. Model SSTA following the application of a (variable-phase-duration) composite MJO  
937 wind stress anomaly.